Novel Enhancement of Energy Management in Fuel Cell Hybrid Electric Vehicle by an Advanced Dynamic Model Predictive Control

Arivoli Anbarasu[a], Truong Quang Dinh[b,*], Somnath Sengupta[c]

[a] *Department of Mechanical Engineering, Indian Institute of Technology Kharagpur, Kharagpur, West Bengal, India*
[b] *Warwick Manufacturing Group (WMG),University of Warwick, Coventry CV4 7AL, UK*
[c] *Advanced Technology Development Center, Indian Institute of Technology Kharagpur, Kharagpur, West Bengal, India*

Abstract

In this paper, an Advanced Dynamic Model Predictive Control (AMPC) based on a Nonlinear Model Predictive Control (NMPC) framework with a multi-objective cost function driven by dynamic weights is proposed to improve the energy performance of fuel cell hybrid electric vehicles whilst prolonging their component lifetime. By the use of dynamic weights, the cost function is effectively formulated as the combination of fuel consumption, rate of change of fuel cell power, battery power, the fuel cell efficiency, state of charge of the battery, and their temperatures. In order to enhance the adaptability of the AMPC, a Fuzzy Cognitive Map (FCM) is then newly designed to regulate online the dynamic weights to adjust the importance of each cost component according to the conditions prevailing during driving. A comparative study between the proposed AMPC, a constant weight based NMPC and a conventional NMPC having cost function with fewer objectives has been carried out by means of simulation using a FCHEV model from the simulation tool ADVISOR to illustrate the efficacy of the proposed AMPC.

Keywords: Fuel Cell Hybrid Electric Vehicle, Energy Management System, Simulink design, Nonlinear Model Predictive Control, Fuzzy Cognitive Map, Fuel cell degradation

1. Introduction

With rising concern over rising global temperature and pollution caused by the use of carbon-based fuels, as well as the depletion of natural fuel reserves at an alarming rate, the world is transitioning toward renewable, green fuels for energy. One of the potential alternatives is hydrogen. Hydrogen is an a ubiquitous element in the universe that may be produced on Earth by electrolyzing water. When hydrogen is combusted (oxidised), the product is water, which is environmentally safe. Many studies are being carried out in the field of hydrogen fuel cells as a transportation power source, with great emphasis to Proton Exchange Membrane Fuel Cells (PEMFC) [1]. PEMFC is the most commonly used fuel cell in the automotive sector due to its advantages such as usage of solid electrolyte, lower operating temperature, faster start-up, and higher efficiency [2, 3]. Even though fuel cells have many advantages, they are not used alone in automobile applications due to the slow response to power demands. The power delivery delay is attributed to the slow dynamics of mechanical valves, pumps present in the hydrogen and oxygen supply line [4]. Fuel cells also cannot absorb energy generated during vehicle braking. Thus, secondary sources such as batteries and/or ultra-capacitors are used in conjunction with fuel cells in order to provide a large amount of power in a short span and absorb the regenerative braking energy [4].

Fuel cell Hybrid Electric Vehicles (FCHEV) are electric vehicles having hybrid power sources, fuel cell and battery. Having hybrid power sources helps to operate the vehicle effectively under different conditions by splitting power between the fuel cell and battery so that both can operate in their high-efficiency regions [5]. This decision of power split is taken by a so-called Energy Management System (EMS). In FCHEVs, the key to success is that an EMS needs to take care of the power split to deal with different decisive factors such as minimization of fuel consumption, braking energy recuperation, efficiency, and safety of the various vehicle sub-systems.

State-of-the-art literature shows that EMS for FCHEV can be broadly classified into two types - rule-based management and optimization-based management [6]. In rule-based management, the controller splits the demanded power between the power sources according to predefined rules created by experts. Deterministic rule-based control techniques such as Thermostat control [7], Power Following control [8], Finite State Machine Control [9] fall under this category. Due to the simple design and low computational demand, these energy management schemes are widely used in commercial applications. However, these controllers perform poorly in real-world

*Corresponding author
Email address: T.Dinh@warwick.ac.uk (Truong Quang Dinh)

Nomenclature

$(\frac{dP_{fc\_FCM}}{dt})_{max/min}$	Limits of rate of fuel cell power given by FCM in AMPC
α_i	Coefficient for the expression of $\dot{m}_{H_2}hot$ (i=1..4)
β_i	Coefficient for the expression of h_{rad} (i=1,2,3)
$\dot{m}_{air}$	Mass flow rate of air across modules of battery
$\dot{m}_{cabin}$	Mass flow rate of air in cabin
$\dot{m}_{H_2hot}$	Mass flow rate of fuel in hot condtitions
η_{cabin}	Efficiency of cabin heat transfer
γ_i	Coefficient for the expression of v_{htx} (i=1,2,3)
θ	Angle of elevation
θ_{FCM}	Bias of threshold function in FCM
A	Frontal area of vehicle
a	Acceleration of the vehicle
A_i	Input concepts of Fuzzy Cognitive Map (i=1..9)
$A_{frontal}$	Frontal area of the radiator
C_d	Drag Coefficient
$c_{rolling}$	Rolling friction coefficient
Cp_{air}	Heat capacity of air
Cp_{fc}	Heat capacity of fuel cell
Cp_{module}	Heat capacity of module of battery
g	Acceleration due to gravity
h_{rad}	Heat transfer coefficient of radiator
LHV	Lower Heating Value of fuel
m_v	Mass of vehicle
m_{fc}	Mass of fuel cell
m_{module}	Mass of each module of battery
n_{module}	Number of modules in battery
P_{demand}	Power demanded by the vehicle
$P_{fc}^{command}$	Fuel cell power command
P_{fc}^{prev}	Previous fuel cell power
r	Radius of the wheel
T_{air}	Temperature of air surrounding the battery
T_{amb}	Ambient temperature
T_{b_ref}	Battery reference temperature
T_{fc_max}	Maximum fuel cell temperature
$t_{fc\_min\_off}$	Minimum fuel cell off time
$t_{fc\_min\_on}$	Minimum fuel cell on time
T_{fc_ref}	Fuel cell reference temperature
tf	Temperature correction factor for $\dot{m}_{H_2hot}$
$u_{working\_min}$	Minimum fuel cell working power
v	Velocity of the vehicle
v_{htx}	Air velocity in the radiator
W_i	Weights of NMPC cost function (i=1..7)
T	Sampling time interval for the controller

driving situations since the rules are dependent on the designer's expertise and are created for a limited number of driving scenarios. Fuzzy rule-based control strategies [10, 11] are an improvement compared to deterministic rule-based control strategies due to the decision making mechanism, which mimics the way of human thinking to control the power split. Nevertheless, fuzzy-based approaches require more design effort and only adapt to a limited range of system uncertainties. Hence, this kind of energy management is not robust to unseen disturbances.

Meanwhile, optimization-based management is used where the power split is done by minimizing an objective function. In [12], a comparative study between rule-based and optimization-based energy management systems for heavy duty fuel cell vehicles has been carried out by means of simulation to confirm the superior performance of optimization-based EMS. Optimization-based EMS is further classified into two types: online EMS and offline EMS [5]. Offline optimization techniques such as Dynamic programming [13–16], Genetic Algorithm [17] require information about the complete trip and external disturbances to derive a globally optimal solution which can be used as reference of power split during the vehicle operation [5]. Since driving conditions are normally unknown and these techniques require significant computational effort, their direct implementation is impractical; thus, online-based EMS is a preferable option. With

online EMS methods, an objective function is optimized in real-time to obtain the control input in-situ without the full drive cycle knowledge. Such optimization provides a sub optimal solution by predicting the system states in the near future, such as Model Predictive Control [18, 19] or by considering future system conditions in evaluating the current power split. Equivalent Consumption Minimization Strategy (ECMS) [20–22] and Pontryagin's Minimum Principle (PMP) [23] comes under latter. PMP provides an optimal solution by minimizing a Hamiltonian. Although PMP is capable of providing solutions comparable to Dynamic Programming, it requires tuning of co-state in the Hamiltonian for different driving conditions to obtain an optimal solution. ECMS derives the power split between various power sources at each instant by optimising an equivalent energy consumption of the vehicle using equivalent factors. Similar to PMP, to enhance the optimal operation of ECMS requires tuning the equivalent factor for different operating modes, which is difficult unless information about the driving condition is available. Meanwhile, MPC is a receding horizon control method that optimizes the system's future state by using predictions from the system's dynamic model and control variables. Only the first control variable obtained from the optimal control policy is then utilized in the current step, while the remainder is discarded. The prediction horizon is shifted one step forward, and the process is repeated for the next step. Due to the ability to deal with multiple objectives, MPC is known as a feasible solution for process control [24] and energy management for hybrid electric vehicles [25–27]

MPC techniques employed for EMS application can be classified as linear and nonlinear. Different to linear MPC which uses linearized equations of the plant, nonlinear MPC (NMPC) offers better performance using nonlinear models which can capture the dynamics of the plant effectively. In [28], a recurrent neural network is used as a fuel cell prediction model to construct the NMPC-based energy management for FCHEVs. Incorporating power source degradation into the prediction model is critical for developing health-conscious EMS. Because of its ability to handle non-linear prediction models, NMPC can efficiently handle power source deterioration models. In [29] a NMPC with highly nonlinear battery degradation model was employed in the EMS of a hybrid electric vehicle. The health conscious EMS improved the fuel consumption and battery life compared to the EMS not considering the degradation of battery. In [30], the authors have employed degradation models of the fuel cell and battery in the NMPC based EMS for FCHEV. The results show that considering the health of the power sources in EMS can lead to lower operating costs. NMPC also permits the use of nonlinear cost functions in the optimization, allowing the use of nonlinear economic stage cost incurred in the plant, multiple objective oriented minimizing function as cost function [31]. In [30, 32] the monetary cost associated with the operation of FCHEV is taken as the cost function to be minimized in NMPC. The cost function includes the cost of hydrogen, cost incurred due to fuel cell and battery degradation. In another study [33], a multi objective cost function, dealing with fuel cell power tracking, battery state of charge set point tracking and fuel cell power regulation is proposed to reduce fuel cell power fluctuation and minimal fuel consumption via state of charge of the battery tracking.

To improve the prediction of NMPC, velocity predictors can be used in conjunction with NMPC. In [33], an online learning Markov speed predictor is used in conjunction with an MPC based on a multi objective cost function. The predicted velocities from the online learning Markov predictor is then used to create a state of charge reference. The velocity predictors are utilised in recent literature to characterise future driving conditions based on expected velocity and acceleration. Then the classification is used to choose the mode of operation of EMS. In [34], the online driving condition is classified using a probabilistic driving cycle classification approach based on three driving conditions. By using data fusion approach, the probability distribution is used to calculate online the parameters of the three offline tuned fuzzy logic controllers which drive the decision-making of the EMS. Utilising the similar concept, a NMPC-based EMS with an adaptive cost function is proposed [35, 36]. The cost function's weights are selected online from predefined sets of weights generated for various driving conditions. To identify the online driving condition, a Markov pattern recognizer is utilised.

However, the above literature study identified limitations in the literatures and opportunities for improvement in NMPC-based EMS for FCHEV, which are listed below:

1. The need of complex vehicle model, sub-system model or artificial intelligence-based black-box models to enable the optimisation require significant time and effort to develop. In addition, training and/or parametrising these models for diverse working conditions, especially for life prediction, necessitates the collection of energy system data for various conditions, which is time consuming and laborious [28, 29].
2. Using monetary cost in the cost function requires extra effort in setting the weights of cost components that cannot be assigned comparable monetary cost, such as set point tracking of battery state of charge, as seen in [30, 32].
3. The temperature conditions of the fuel cell and battery are not taken into account in the EMS decision ([33, 35, 36]). Maintaining the temperatures of the fuel cell and battery is critical for optimal performance with minimal deterioration [30].
4. The identification of driving cycles and/or modes can occasionally be incorrect, potentially causing poor

performance of EMS. Switching the EMS modes or regulating the EMS cost functions based on driving pattern recognition on a frequent basis might impair the EMS's efficiency [7, 34, 35].

To address the aforementioned research problems, an advanced NMPC based on a dynamic multi-objective cost function (named as AMPC) is proposed in this study for efficient energy management of FCHEVs. The contribution of this work can be expressed as follow:

1. Different from [28], only a simple plant model of the fuel cell is required for the design of AMPC. Here, the AMPC will consider the state of charge of the battery, temperatures of fuel cell and battery, power demand as the measurement inputs to derive the optimal power command of the fuel cell and battery.
2. Different from [30, 32, 33], the AMPC cost function is designed to address all aspects of energy management in FCHEVs using dynamic weights. The goal is to minimise the fuel consumption and maintain the battery state-of-charge, but also to prevent the power sources' deterioration due to a variety of factors. In addition, objectives associated with the optimal temperature operating regions of the power sources are integrated in this design via activation functions.
3. Different from existing studies on enhancing the adaptability of NMPC [35, 36], a novel continuous weight regulation method is proposed to regulate online the AMPC cost function weights by considering only the vehicle instantaneous states and power demand.
   (a) The cost components are normalised according to their ranges to minimise the design and calibration efforts.
   (b) A fuzzy cognitive map architecture is designed based on the dynamic relationship between the AMPC cost function weights and vehicle states, allowing for easy calibration and transparency in the relationship between the states and the weights.
   (c) Therefore the AMPC cost function weights can be directly regulated based on an instant update of vehicle states without the need of driving condition recognition.
4. A comparative study between the AMPC and a typical NMPC has been carried out by means of simulations under different driving scenarios to confirm the superiority of the proposed approach.

The rest of the paper is organized as follows: the FCHEV architecture and its dynamic model are introduced in Section 2; the design of NMPC framework, cost function, constraints and the FCM for the AMPC is presented in Section 3 while the simulation study on the AMPC using the FCHEV model is presented in Section 4; the conclusions and future work are finally given in Section 5.

2. System Architecture and Dynamics

The architecture of the studied FCHEV is depicted in Figure 1a. A unidirectional DC/DC booster is employed to ensure voltage matching between the fuel cell and the battery [4]. The motor takes in power from the battery and fuel cell through an inverter. The torque generated from the motor is then transferred to the wheels via the drivetrain. Here, the parallel architecture of the power sources enables the following modes:

1. Traction using both the fuel cell and battery
2. Traction using only the fuel cell. Once necessary, the battery can be charged in this case using redundant power generated by the fuel cell
3. Traction using only the battery
4. Braking with/without regeneration. The braking energy can be utilised to charge the battery under its constraints, such as SoC, temperature and maximum charge current.

The selection of above modes as well as decision on power distribution between the fuel cell and battery are derived by the EMS based on the measured vehicle states. Without loss of generality, only longitudinal vehicle dynamics are considered in this study. Based on [5], the vehicle traction torque and angular speed of wheels can be calculated using Equation 1.

$$\begin{aligned} T_v &= (m_v g c_{rolling} cos(\theta) + 0.5\rho A C_d v^2 + m_v a + m_v g sin(\theta))r \\ \omega_v &= \frac{v}{r} \end{aligned} \tag{1}$$

The gearbox in the drivetrain uses a single gear ratio (gr) to amplify the torque produced by the motor. The relationship between wheel torque and speed to the input torque and speed to the gear box considering efficiency (η_{gb}) is as shown in Equation 2

$$\begin{aligned} \omega_{gb} &= (gr)\omega_v \\ T_{gb} &= \begin{cases} \frac{T_v}{(gr)\eta_{gb}} & T_v \geq 0 \\ \frac{\eta_{gb} T_v}{gr} & T_v < 0 \end{cases} \end{aligned} \tag{2}$$

The connection between gear box and motor is assumed to be ideal. Therefore the motor speed (ω_m) and torque (T_m) is equal to ω_{gb} and T_{gb} respectively.

2.1. Fuel Cell

A fuel cell is a type of electrochemical device that transforms chemical energy into electrical energy. During the operation of a PEMFC system in FCHEV, hydrogen (from pressurized storage) oxidizes in the anode releasing electrons and protons. Protons are allowed to flow through the solid membrane, but electrons are not permitted and must travel through an external circuit [3]. The protons from the anode reaches the cathode and reacts with oxygen (from atmosphere, pressurized by compressor) to produce

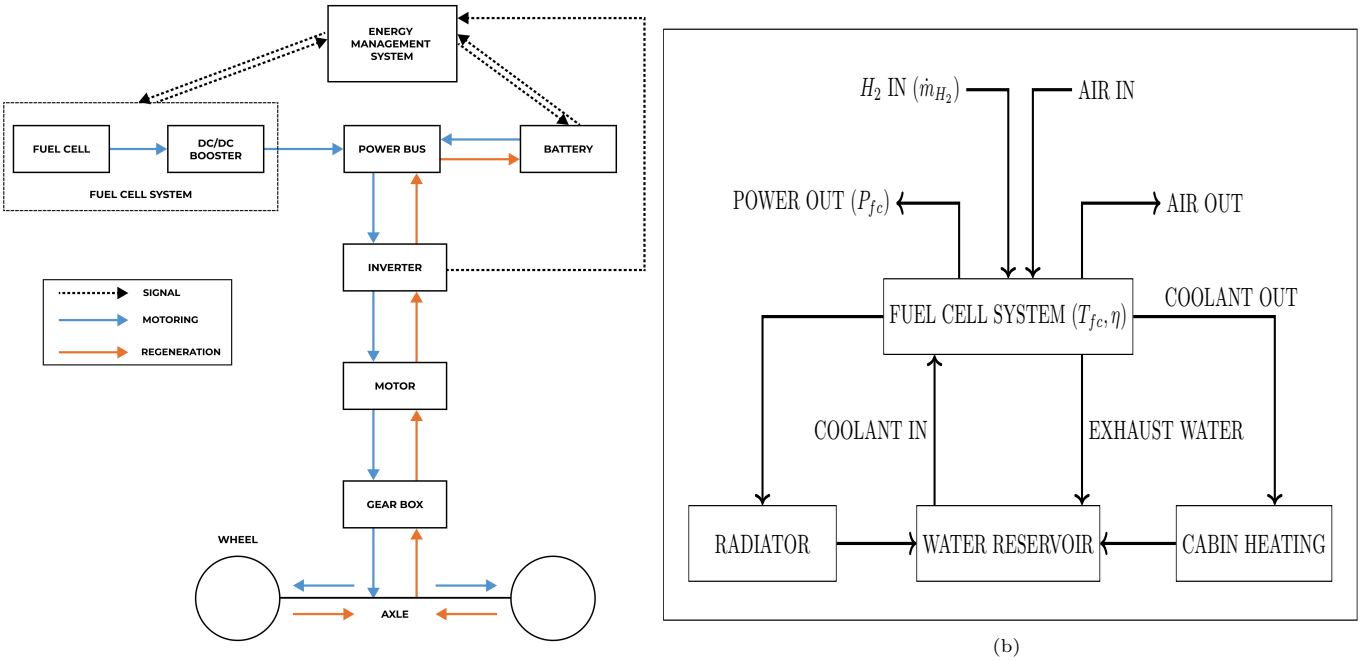

(a) (b)

Figure 1: (a) Power Flow and signal flow in FCHEV under different conditions (b) Process flow diagram of the Fuel Cell system [38]

water. The electrical power generated by the fuel cell system is used to power the vehicle. The water produced in the chemical reaction is returned to a reservoir. The heat generated during the chemical process is removed from the fuel cell by using a cooling system as shown in Figure 1b. Here, the deionized water from the reservoir is used as the coolant to maintain the temperature of the fuel cell and humidity in the membrane (the heat is dissipated via the cabin and radiator).

The rate of hydrogen consumed by the fuel cell can be represented as a polynomial function of net fuel cell power. The coefficients of the polynomial approximating the rate of hydrogen consumption in Equation 3 $(\alpha_1, \alpha_2, \alpha_3, \alpha_4)$ can be derived from the measurements of rate of hydrogen consumption during fuel cell operation. Because the measurements for the rate of hydrogen consumption are conducted at high temperatures, a correction factor is further applied to account for higher fuel consumption at lower temperatures [37]. The expression for temperature-corrected fuel consumption rate $(\dot{m}_{H_2})$ is therefore given in Equation 3.

$$\begin{aligned} \dot{m}_{H_2hot} &= \alpha_1 P_{fc}^3 + \alpha_2 P_{fc}^2 + \alpha_3 P_{fc} + \alpha_4 \\ tf &= 1 + 0.1((T_{fc\_max} - T_{fc})/(T_{fc\_max} - T_{amb}))^{0.65} \\ \dot{m}_{H_2} &= \dot{m}_{H_2hot} tf \end{aligned} \tag{3}$$

The thermal model of the fuel cell system is modelled under the assumption that the fuel cell temperature and coolant temperature are the same and denoted by T_{fc} and radiator heat transfer $Q_{radiator}$ happens only when fuel cell temperature exceeds its cutoff temperature. The heat generated by the fuel cell and the heat transfer between coolant and surrounding are then described as in Equation 4.

$$\begin{aligned} Q_{generated} &= \dot{m}_{H_2} LHV - P_{fc} \\ Q_{cabin} &= \eta_{cabin} \dot{m}_{cabin} Cp_{air} (T_{fc} - T_{amb}) \\ Q_{radiator} &= h_{rad} A_{frontal} (T_{fc} - T_{amb}), if\ T_{fc} > T_{fc\_cutoff} \\ Q_{coolant} &= Q_{cabin} + Q_{radiator} \end{aligned} \tag{4}$$

The heat transfer coefficient h_{rad} can be calculated from air velocity in the radiator v_{htx} using an empirical model as presented in Equation 5 ([39]). Here, the air velocity in the radiator can be represented as a function of vehicle velocity. Meanwhile, the heat transfer model coefficients $(\beta_1, \beta_2, \beta_3)$ can be derived from the data obtained through heat transfer measurements between the radiator and air [40] and the air velocity model coefficients $(\gamma_1, \gamma_2, \gamma_3)$ can be derived from the data obtained from wind tunnel tests [41].

$$\begin{aligned} h_{rad} &= \beta_1 v_{htx}^2 + \beta_2 v_{htx} + \beta_3 \\ v_{htx} &= \begin{cases} (\gamma_1 v^{\gamma_2} + \gamma_3) v & if\ v > 1\,\mathrm{m/s} \\ 5.073 v & else \end{cases} \end{aligned} \tag{5}$$

Using Equation 4, Equation 5, the dynamic equation of Fuel Cell temperature T_{fc} is obtained. The fuel cell tem-

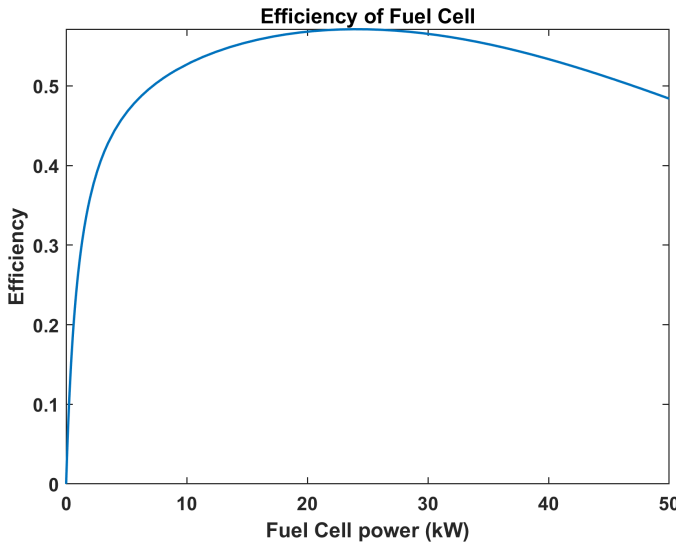

Figure 2: Efficiency of Fuel Cell as a function of Output power [37]

perature can be computed using Equation 6.

$$\dot{T}_{fc} = \frac{Q_{generated} - Q_{coolant}}{m_{fc} Cp_{fc}} \tag{6}$$

The efficiency of the fuel cell is calculated as the ratio of net output power to the available power in the fuel. Using the mass flow rate of hydrogen in Equation 3, the efficiency of the fuel cell is calculated in Equation 7.

$$\eta = \frac{P_{fc}}{\dot{m}_{H_2} LHV} \tag{7}$$

Figure 2 then demonstrates an efficiency curve of a PEMFC system with maximum power output of 50kW as a function of the output power [37]. As seen in this figure, around half of the power generated in a fuel cell could be lost. This loss mainly comes from the heat generated in the fuel cell due to reactions and ohmic loss in the fuel cell. In addition, a small fraction of the energy generated is used to run auxiliary systems (such as air compressor, coolant pump, and fans) to provide suitable operating conditions for the fuel cell [38]. Therefore, it is important for the EMS to consider the efficiency of fuel cell in its decisions to maximise the fuel cell efficiency.

Next, transient dynamics of the fuel cell during start-up or power changing phase is considered. To represent the slow response of the fuel cell in these scenarios, a low pass filter with time constant t_s is included in the fuel cell model. The fuel cell output power can be then represented by Equation 8.

$$P_{fc} = P_{fc}^{command} \frac{T}{t_s + T} + P_{fc}^{prev} \frac{t_s}{t_s + T} \tag{8}$$

Another important issue when using fuel cells is degradation, since it affects the operating lifetime. An efficient management of fuel cell operation can increase the life of the fuel cell, enabling the minimisation of its life-cycle cost. The operational factors that contribute to the degradation of FC are primarily divided into four categories [30],[42] :

1. **Frequent start/stop:** Large number of start/stop of fuel cell results in inadequate reactants inside the membrane electrode assembly resulting in starvation of reactants.
2. **Low power operation:** Operating at power lower than 20% of rated power leads to formation of surface oxides.
3. **High power operation:** At higher power (higher than 80%) [32], heat generation is large, leading to high temperatures in fuel cell. Higher temperatures can create thermal stress, accelerate reactions and reduce humidity in the membrane thus reducing ion conduction in membrane.
4. **Transient loading:** Continuous change in operating point of fuel cell can lead to reactant starvation which causes carbon electrodes to oxidize.

The total deterioration in the voltage of fuel cell can be determined using Equation 9 and Table 1, assuming that each factor's contribution to degradation is independent of each other [43].

$$V_{degrade} = \gamma_{low} t_{low} + \gamma_{high} t_{high} + \gamma_{transient} \Sigma \left| \frac{dP_{fc}}{dt} \right| + \gamma_{cycle} n_{cycle} \tag{9}$$

The fuel cell's state of health is used to calculate its lifetime as follows:

Table 1: Degradation Rate for PEMFC (per cell) [42]

Condition	Degradation Rate
Low power Operation (γ_{low})	10.17 µV/h
High Power Operation (γ_{high})	11.74 µV/h
Transient Loading ($\gamma_{transient}$)	0.0441 µV/kW
Start/Stop (γ_{cycle})	23.91 µV/cycle

$$SOH = 1 - \frac{V_{degrade}}{V_{maxdrop}} \tag{10}$$

where, $V_{maxdrop}$ is the maximum fuel cell voltage drop at the end of life of fuel cell [22].

2.2. Battery

Lithium-ion based batteries are widely employed as energy storage systems in FCHEV because of their longer life cycle [44]. Because of its easy and realistic depiction of data, the internal resistance model is employed for lithium-ion battery simulation [3]. As illustrated in Figure 3, the internal resistance model of the battery consists of an ideal cell with open-circuit voltage Voc and internal resistance $Rint$ in series with the cell. The internal resistance of the battery varies depending on whether it is

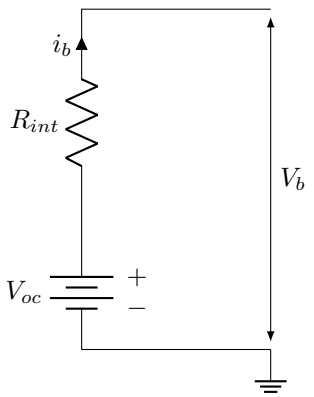

Figure 3: Internal resistance model of battery

charging or discharging [3]. The battery's output power (P_b), terminal voltage (V_b) and current (i_b) can be related by Equation 11.

$$\begin{aligned} P_b &= V_{oc} i_b - R_{int} i_b^2 \\ i_b &= \frac{V_{oc} - \sqrt{V_{oc}^2 - 4P_b R_{int}}}{2R_{int}} \\ V_b &= V_{oc} - R_{int} i_b \\ V_b &= \frac{V_{oc} + \sqrt{V_{oc}^2 - 4P_b R_{int}}}{2} \end{aligned} \tag{11}$$

The amount of energy stored in the battery is quantified by calculating the amount of charge left in the battery for usage. The amount of available charge to the maximum charge capacity of the battery is referred to as the State of Charge (SoC) of the battery [45]. The Coulombic Efficiency (C_{eff}) is used to quantify the effect of charging loss. The dynamic equation for the state of charge of the battery during charging and discharging is given by Equation 12 [45].

$$\dot{soc} = \begin{cases} -\frac{i_b}{C_{Ah}} & i_b \geq 0 \\ -\frac{C_{eff} i_b}{C_{Ah}} & i_b < 0 \end{cases} \tag{12}$$

where C_{Ah} is the maximum capacity of the battery. The equations of Open Circuit Voltage (V_{oc}), Internal Resistance of the battery (R_{int}) for charging and discharging condition, Coulombic efficiency (C_{eff}) and Maximum capacity of the battery (C_{Ah}) as a function of SoC and battery temperature T_b are provided in Appendix A.

The thermal performance of the battery with air cooling can be represented by a lumped capacity model [46]. The heat generated by Joule heating and Coulombic inefficiency Q_{b_gen} is absorbed by the air through convection. For temperatures below cutoff temperature, surrounding air gets heated, and fresh air gets replenished. When the temperature rises above the cutoff point, a fan turns on. Due to forced convection, it is assumed that 50% of heat absorbed by air is convected away while 50% of heat absorbed results in heating of air [46]. The heat absorbed by the air is denoted by Q_{b_air}. After air cooling, the net heat generated is as illustrated in Equation 13.

$$\begin{aligned} Q_{b\_gen} &= \begin{cases} i_b^2 R_{int} - V_b i_b (1 - C_{eff}) & , if\ i_b < 0 \\ i_b^2 R_{int} & , else \end{cases} \\ Q_{b\_air} &= \begin{cases} \frac{T_b - T_{air}}{R_{on}}, if\ T_b \geq T_{b\_cutoff} \\ \frac{T_b - T_{amb}}{R_{off}}, if\ T_b < T_{b\_cutoff} \end{cases} \\ T_{air} &= T_{amb} + \frac{0.5 Q_{b\_air}}{\dot{m}_{air} Cp_{air}}, if\ T_b \geq T_{b\_cutoff} \\ q_b &= \frac{Q_{b\_gen} - Q_{b\_air}}{n_{module}} \end{aligned} \tag{13}$$

where, T_b is the temperature of the battery and SoC is the State of Charge of the battery. R_{on}, R_{off} are the effective thermal resistance when airflow is present and absent respectively. The rate of change in battery temperature is calculated using Equation 14.

$$\dot{T}_b = \frac{q_b}{m_{module} Cp_{module}} \tag{14}$$

2.3. Electric Motor

The electric motor is an important component of the FCHEV. The machine converts electrical energy into mechanical energy to be provided to the wheels and vice versa. In this paper, an AC induction motor and an inverter are employed. Curve fitted equations for maximum torque and electrical power considering the efficiency of the inverter are provided in Appendix B

3. Advanced NMPC Design Formulation for Energy Management

The fundamental goal of an Energy Management System is to coordinate the fuel converter and energy storage systems to supply the motor with the required power. However, an EMS's strength resides in achieving the primary purpose while lowering the cost of vehicle operation. The cost of operation can be reduced by lowering fuel usage and extending the vehicle's life. FCHEV's operating costs can be reduced by

1. Minimizing Fuel Consumption (m_{H_2}).
2. Minimizing Battery Energy Consumption ($\int P_b dt$).
3. Operating Fuel Cell at its efficient point (η).
4. Maintaining Fuel Cell temperature T_{fc} in the optimum range.
5. Operating the battery at or near its nominal State of Charge to prevent deep discharge and ensuring sufficient capacity is available for regeneration power.
6. Maintaining Battery Temperature T_b in the optimum range.

7. Minimizing the degradation of the fuel cell by avoiding situations that accelerate the degradation as seen in Table 1.

The first three aims are concerned with reducing fuel consumption, while the last four objectives are concerned with extending the life of FCHEV. The fuel cell and battery dynamics and the thermal dynamics involved are highly nonlinear and cannot be retained by utilizing linear time-varying MPC. To deal with this design challenge, the Advanced Dynamic Model Predictive Control (AMPC) based on the NMPC framework is introduced in this section.

3.1. NMPC Formulation

Nonlinear Model Predictive Control (NPMC) is an optimization-based feedback control technique. The cost function is optimized for a finite time horizon in the future, known as the prediction horizon. The future states are predicted using current state measurements and a dynamic model of the system [31]. For Energy Management problem in FCHEV, the control problem is formulated as

$$\min_{u(k),u(k+1)..u(k+N-1)} J(k) \tag{15}$$

where,

$$J(k) = \sum_{i=0}^{N-1} \{C_{stage}(x(i|k), u(i|k), u_m(i|k))\} + C_{terminal}(x(N|k)) \tag{16}$$

Such that,

$$x(k+1) = g(x(k), u(k), u_m(k)), x \in \mathbb{X},\ u \in \mathbb{U} \tag{17}$$

$$h(x(k), u(k), u_m(k)) \leq 0 \tag{18}$$

$$m(x(k), u(k), u_m(k)) = 0 \tag{19}$$

The cost component C_{stage} represents the stage cost to be minimized inside the prediction horizon. The terminal cost $C_{terminal}$ is added to the total cost function $J(k)$ at the end of the prediction horizon. Terminal cost is used in the formulation of cost function to stabilize the optimization problem [31]. Manipulated or control variable is chosen as the Fuel cell power $u(k) = P_{fc}(k)$. The state vector for the optimal control problem is defined as $x(k) = [soc(k), T_{fc}(k), T_b(k)]$. Exogenous input vector contains information required for solving the optimization problem $u_m(k) = [P_{demand}(k), fc\_on(k-1), v(k-1), P_{fc}(k-1)]$

The state updation rule in discrete form $x(k+1) = g(x(k), u(k), u_m(k))$ is obtained by integrating the continuous state space equation $\dot{x} = f(x(k), u(k), u_m(k))$. The continuous state space equations can be constructed from the dynamic equations of State of Charge (Equation 12), Fuel cell temperature (Equation 6), Battery temperature (Equation 14). $m(x(k), u(k), u_m(k)), h(x(k), u(k), u_m(k))$ are respectively the equality and inequality constrains to be followed during optimization.

3.2. Cost formulation for AMPC

To address all the objectives described above, a cost function comprising multiple objectives is formulated. The prediction horizon stage cost C_{stage} is constructed based on the seven objectives defined above. Equation 20 depicts the components of C_{stage}

$$\begin{aligned} \underset{k=0,1,\ldots N-1}{C_{stage}(k)} &= C_{m_{H_2}}(k) + C_{P\_batt}(k) + C_{fc\_rate}(k) \\ &+ C_{fc\_eff}(k) + C_{soc}(k) + C_{T_{fc}}(k) + C_{T_b}(k) \end{aligned} \tag{20}$$

where,

$$C_{m_{H_2}} = W_1 (\frac{\dot{m}_{H_2}}{\dot{m}_{H_2 max}})^2 \tag{21}$$

$$C_{P\_batt} = W_2 \frac{P_b}{P_{b\_max}} \tag{22}$$

$$C_{fc\_rate} = W_3 (\frac{P_{fc}(k) - P_{fc}(k-1)}{\dot{P}_{fc\_max} T})^2 \tag{23}$$

$$C_{fc\_eff} = \begin{cases} 0 & , if\ P_{fc} = 0 \\ W_4 (\frac{\eta - \eta_{max}}{\eta_{max}})^2 & , else \end{cases} \tag{24}$$

$$C_{soc} = W_5 (\frac{2(soc - soc_{nom})}{soc_{max} - soc_{min}})^2 \tag{25}$$

$$C_{T_{fc}} = \begin{cases} W_6 (\frac{T_{fc} - T_{fc\_ref}}{T_{fc\_max} - T_{fc\_ref}})^2 & , if\ T_{fc} > T_{fc\_ref} \\ 0 & , else \end{cases} \tag{26}$$

$$C_{T_b} = \begin{cases} W_7 (\frac{T_b - T_{b\_ref}}{T_{b\_max} - T_{b\_ref}})^2 & , if\ T_b > T_{b\_ref} \\ 0 & , else \end{cases} \tag{27}$$

here, all the cost factors are written in their normalised forms to minimise the calibration efforts. Particularly, $C_{m_{H_2}}$ relates to the minimization of hydrogen mass flow rate; C_{P_batt} is designed to minimize battery power at each step; the rate of change of fuel cell power is minimized using C_{fc_rate}; C_{fc_eff} encourages the fuel cell to operate near the maximum efficiency region and it is active only when the fuel cell is on; C_{soc} is utilized to keep SoC close to its nominal value (the average of soc_{max} and soc_{min}); $C_{T_{fc}}$ and C_{T_b} are designed to penalized the controller when the temperature crosses their respective reference temperatures. The weights $W_1 - W_7$ are tuned to get the best performance of the EMS. The weights indicate the relative significance of each of the above mentioned cost components. Next, a terminal cost $C_{terminal}(N)$ with weight $w_{terminal}$ is used in the optimization to enforce the set point tracking of soc (Equation 25), T_{fc} (Equation 26) and T_b (Equation 27). The formulation of terminal cost is shown in Equation 28.

$$C_{terminal}(N) = w_{terminal}(C_{soc}(N) + C_{T_{fc}}(N) + C_{T_b}(N)) \tag{28}$$

3.3. Constraints

The physical constraints of the fuel cell and battery are expressed as equality and inequality equations used during cost function optimization. The drivability of the vehicle must be maintained at all times. First, the power demanded by the vehicle must be satisfied by the power sources:

$$P_{total} = P_{motor} + P_{accessory} = P_{fc} + P_b \tag{29}$$

Next, the fuel cell power is limited by maximum allowable power limit. Since the fuel cell cannot absorb energy, its minimum power is set as zero. The temperature of the fuel cell must not exceed the maximum limit. Meanwhile, the rate of change of fuel cell power is limited to reduce deterioration due to transient loading [43]:

$$P_{fc\_min} \leq P_{fc} \leq P_{fc\_max} \tag{30}$$

$$(\frac{dP_{fc}}{dt})_{min} \leq \frac{dP_{fc}}{dt} \leq (\frac{dP_{fc}}{dt})_{max} \tag{31}$$

$$T_{fc\_min} \leq T_{fc} \leq T_{fc\_max} \tag{32}$$

To reduce frequent switching of the fuel cell, a minimum switch off/on duration for the fuel cell is used in the EMS [2]. The fuel cell must maintain power above a particular threshold value, called $u_{working\_min}$ if the time period between turning on the fuel cell and turning it off (Δt_{on}) is less than the *minimum fuel cell on duration* ($t_{fc\_min\_on}$) and the fuel cell must remain off, if the time it has been off from the preceding on (Δt_{off}) is less than the *minimum fuel cell off duration* ($t_{fc\_min\_off}$).

$$P_{fc} \geq u_{working\_min} \qquad if\ \Delta t_{on} \leq t_{fc\_min\_on} \tag{33}$$

$$P_{fc} = 0 \qquad if\ \Delta t_{off} \leq t_{fc\_min\_off} \tag{34}$$

Finally, the battery's state of charge, output power, terminal voltage, and temperature must remain within their bounded limits to operate the battery safely and efficiently:

$$soc_{min} \leq soc \leq soc_{max} \tag{35}$$

$$P_{b\_min} \leq P_b \leq P_{b\_max} \tag{36}$$

$$V_{b\_min} \leq V_b \leq V_{b\_max} \tag{37}$$

$$T_{b\_min} \leq T_b \leq T_{b\_max} \tag{38}$$

The dynamic weight regulation scheme for AMPC based on Fuzzy Cognitive Map (FCM) is described in the following subsection. It is used to regulate the weights of the NMPC cost functions $W_1 - W_7$ according to the instantaneous vehicle states.

3.4. Fuzzy Cognitive Map for AMPC

Fuzzy Cognitive Maps (FCMs) are directed graph-based Fuzzy inference systems [47]. They consist of *concepts* (nodes) and weights associated with each edge connecting the nodes. The weight between ith concept and jth concept $w_{ij} \in [-1, 1]$ specifies the causal relationship between them. A positive weight represents a *proportional relationship* between the concepts, while a negative weight signifies the *inverse relationship*. An example Fuzzy Cognitive Map is shown in Figure 4. Fuzzy Cognitive Maps are preferred over the traditional rule-based fuzzy logic because of their numerical inference based method. The relationship between input and output can be understood intuitively [48] and tuning of fuzzy inference system are easier compared to conventional fuzzy logic. In addition, if the number of inputs increases, the number of rules in traditional fuzzy logic increases many folds, whereas, in FCM, an increase in concepts leads to a slight increase in the number of edge weights. Fuzzy Cognitive Map also has the capability of assigning hidden causality between concepts [49]. Due to the ease of building and tuning FCMs, they are suitable for modelling of physical system [50], functioning as controller [51] and especially functioning as decision making tool [52]. A FCM inference is made in three steps

1. **Concept Updation Rule:** At each time step, concept values (A_i) are either obtained as input (activated concepts)[49] or as previous concept values. These concepts are updated by adding weighted sum of incoming concepts to its predecessor value as seen in Equation 39.

$$A_i^{k+1} = f(A_i^k + \sum_{j=1}^{N} w_{ij} A_j^k) \tag{39}$$

2. **Threshold:** To avoid the value of concepts exceeding the limit of [0,1], a threshold function is used. For our requirement, sigmoid function as defined in Equation 40 is used.

$$f(x) = \frac{1}{1 + e^{-c(x+\theta_{FCM})}} \tag{40}$$

3. **Iteration:** The above two step are repeated until the difference in concept value at iteration k and $k+1$ is lower than δ, $A_i^{k+1} - A_i^k \leq \delta$, where δ is a small positive value.

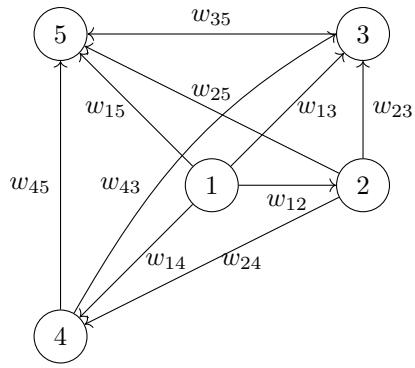

Figure 4: An example of Fuzzy Cognitive Map

Table 2: Definition of Concepts

Concept	Definition
$A_1(soc)$	$\frac{2(soc-soc_{nom})}{soc_{max}-soc_{min}}$,Normalized state of charge of the battery.
$A_2(T_{fc})$	$\frac{T_{fc}-T_{fc\_ref}}{T_{fc\_max}-T_{fc\_ref}}$ if $T_{fc} > T_{fc\_ref}$, Normalized fuel cell temperature.
$A_3(T_b)$	$\frac{T_b-T_{b\_ref}}{T_{b\_max}-T_{b\_ref}}$ if $T_b > T_{b\_ref}$, Normalized battery temperature.
$A_4(t_{hot})$	$\frac{t(T_{fc}>T_{fc\_cutoff})}{t(T_{fc}>T_{fc\_ref})}$, Normalized duration for which $T_{fc} > T_{fc\_cutoff}$.
$A_5(V_{transient})$	$\frac{w_{degrade}\Sigma\lvert\frac{dP_{fc}}{dt}\rvert\gamma_{transient}}{V_{maxdrop}}$, Ratio of degradation due to transient to max degradation.
$A_6(V_{low})$	$\frac{w_{degrade}t(P_{fc}<0.2P_{fc\_max})\cdot\gamma_{low}}{V_{maxdrop}}$, Ratio of degradation due to low power to max degradation.
$A_7(V_{high})$	$\frac{w_{degrade}t(P_{fc}>0.8P_{fc\_max})\gamma_{high}}{V_{maxdrop}}$, Ratio of degradation due to high power to max degradation.
$A_8(V_{cycle})$	$\frac{w_{degrade}n_{cycle}\gamma_{cycle}}{V_{maxdrop}}$, Ratio of degradation due to frequent start/stop to max degradation.
$A_9(V_{degrade})$	Increment in component A_5 in the last 60 seconds.
$A_{10}(W_1)$	Weight corresponding to fuel consumption rate.
$A_{11}(W_2)$	Weight corresponding to Battery Power.
$A_{12}(W_3)$	Weight corresponding to rate of change of fuel cell power.
$A_{13}(W_4)$	Weight corresponding to efficiency of fuel cell.
$A_{14}(W_5)$	Weight corresponding to state of charge of battery.
$A_{15}(W_6)$	Weight corresponding to Fuel Cell Temperature.
$A_{16}(W_7)$	Weight corresponding to Battery Temperature.
$A_{17}(W_8)$	Maximum rate of change of fuel cell power. $(\frac{dP_{fc\_FCM}}{dt})_{max} = (1-W_8)(\frac{dP_{fc}}{dt})_{max}$
$A_{18}(W_9)$	Minimum rate of change of fuel cell power. $(\frac{dP_{fc\_FCM}}{dt})_{min} = (1-W_9)(\frac{dP_{fc}}{dt})_{min}$

In this work, a FCM is newly designed for the AMPC by proposing causality between different concepts based on prior relevant knowledge to update the cost function weights, W_i. The concepts are divided into two categories - input concepts and output concepts. The input concepts are updated at each time step by measurements, while the output concepts are updated by inference process as described above. The FCM architecture created is shown in Figure 5. Table 2 shows the definition of all the concepts involved in the FCM design. To ensure correct causality and relative importance of causality weights, the input values are normalised and used as input concepts. The concepts $A_1 - A_4$ are constructed from the states of the vehicle. Once activated, the fuel cell degradation concepts $A_5 - A_8$ are designed to remain active and non-decreasing (Table 2). This enables the determination of the cost function weights while taking into account the history of fuel cell's deterioration. A factor, $w_{degrade}$ is multiplied to the degradation input concept to make the values comparable to other input concepts. The input concept A_9 is used to regulate the rate of change of fuel cell power by evaluating the recent history of transients (in the last 60 seconds). The output concepts W_8, W_9 are obtained from A_9 and they are used to regulate the limits of rate of change of fuel cell power as shown in Table 2. The updated limits of rate of change of fuel cell specified by the FCM $(\frac{dP_{fc\_FCM}}{dt})_{min}, \frac{dP_{fc\_FCM}}{dt})_{max})$ will be applied in Equation 31.

The vital aspect of building FCM is to define the weights between concepts. The connections from input concepts A_i, i={1..9} to output concepts W_j, j={1..9} are created based on the influences which can be described as below

- W_1 is the weight associated with the mass flow rate of fuel. W_1 is increased when the fuel consumption requirement is less. It occurs when the SoC (A_1) is high or the fuel cell temperature (A_2) is high, fuel cell degradation due to high power operation (A_7) is high. When there is a need for fuel cell power, W_1 is reduced. When battery temperature (A_3) rises, fuel cell power is expected to increase to decrease the battery load. When degradation related to low power operation (A_6) increases, W_1 is lowered to increase fuel cell power.

- Weight W_2 is increased when the temperature of battery (A_3) or fuel cell degradation due to low power operation (A_6) increases. When SoC (A_1) is lower than nominal value, W_2 is increased to promote charging.

- Weight W_3 is increased to reduce the rate of change of power. The concept A_5 corresponding to degradation due to transient loading has the most significant impact on W_3. An increase in fuel cell (A_2) and battery (A_3) temperature allows for relaxation in W_3 to increase or decrease freely.

- Weight W_4 corresponding to fuel cell efficiency is increased when SoC (A_1) is low or battery temperature (A_3) is high, and degradation is high

Table 3: Weight Matrix from input concept A_i to output concept W_i

	A_1	A_2	A_3	A_4	A_5	A_6	A_7	A_8	A_9
W_1	0.1	0.5	-0.5	0.5	0.75	-0.5	0.25	1	0
W_2	-0.05	-0.5	0.5	-0.25	-0.75	0.5	0	-0.5	0
W_3	0.1	-0.1875	-0.125	-0.75	1	-0.5	0.25	0	0
W_4	-0.1	-0.25	0.25	-0.5	0.5	1	-0.25	0	0
W_5	$0.1sign(A_1)$	-0.25	0.5	-0.5	-0.5	1	-0.25	0	0
W_6	0	0.375	-0.25	1	0.5	0	0.25	0	0
W_7	0	0.25	0.5	-0.1	0	0.375	-0.25	0.5	0
W_8	0	0	0	0	0	0	0	0	0.25
W_9	0	0	0	0	0	0	0	0	0.25

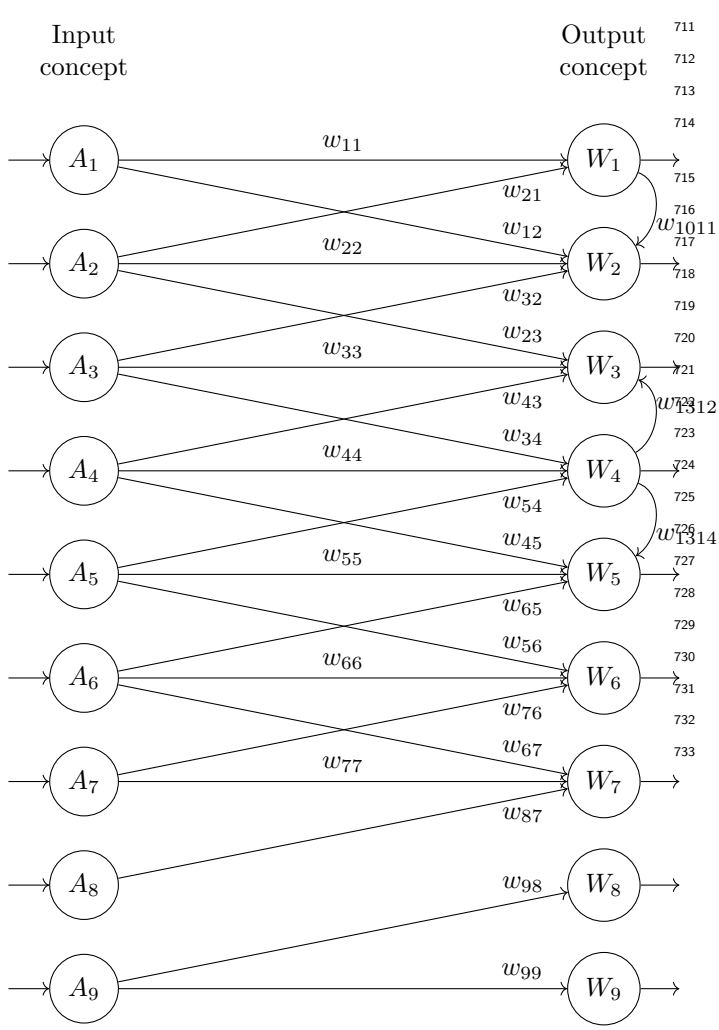

Figure 5: Fuzzy Cognitive Map used for NMPC weight updation

$(A_5, A_6, A_7, A_8, A_9)$. Operating fuel cell at higher efficiency can lead to reduction in degradation [42].

- Weight given to SoC (W_5) increases when SoC (A_1) deviates from nominal value ,temperature of battery rises (A_3) and decreases when fuel cell needs to be taken care of. The connection weight $w_{15} = 0.1sign(A_1)$ is chosen because when $soc > soc_{nom}, A_1 > 0$, thus w_{15} is positive, increasing W_5. Similarly when $soc < soc_{nom}, A_1 < 0$ and $w_{15} < 0$. But the weighted contribution $w_{15}A_1$ is positive thus increasing W_5.

Table 3 shows the causality weight between input concepts and output concepts. This matrix depicts the relationship and the strength of the input on the output concepts. The causality weights are initially tuned based on the incoming concepts A_i and their importance to the output concept W_j. This corresponds to the tuning of causality weights row-wise in Table 3. Then, column-wise tuning of causality weights is done in order to decide the order and weightage of cost function weights for different input concepts. Causality weights between W_i are used to reinforce the importance of the cost function weight compared to other cost function weights. For example, cost function weight W_1 (fuel consumption) is reinforced by cost function weights W_3 (rate of change of fuel cell power), W_4 (fuel cell efficiency), W_5 (SoC), W_6 (fuel cell temperature) by having a positive causality weight, while opposed by cost function weight W_7 (battery temperature) by having a negative causality weight. Table 4 shows the impacts between the output concepts.

Table 4: Weight Matrix from output concept W_i (horizontal) to output concept W_j (vertical)

	W_1	W_2	W_3	W_4	W_5	W_6	W_7
W_1	0	0	0.5	0.1	0.1	0.1	-0.05
W_2	-1	0	0	-0.75	0.05	0	0
W_3	0.5	0	0	0.1	-0.1	0.2	0.1
W_4	0.1	0	0	0	0	-0.1	0.2
W_5	0.3	0	0.2	0.1	0	0	0.05

Using the causality weight matrix, the FCM can provide cost function weights to the NMPC for various combinations of input concepts, thereby covering all driving conditions. Unlike the driving pattern recognizer and fixed cost function weights for each driving mode proposed in [35] the proposed continuous weight regulation method using Fuzzy Cognitive Map is more agile to various driving conditions.

4. Simulation results

In order to evaluate the effectiveness of the designed AMPC, a comparative study between the APMC and other two typical MPC strategies, denoted by MPC-1 and MPC-2, has been carried out by means of simulation. The MPC-1 is a simplified version of the NMPC developed above with fewer components/objectives of the cost function and fixed weights, while the MPC-2 is the NMPC developed in the above section with fixed weights (to be presented later). To support this comparative study, an SUV FCHEV model is created within MATLAB/Simulink environment using ADVISOR (ADvanced Vehicle SimulatOR) [37].

4.1. Simulation environment setup

The created FCHEV model is setup to run in conjunction with the comparative energy management strategies as depicted in Figure 6. In the model, the EMS provides the optimal fuel cell power command to fuel cell and the battery power is calculated by subtracting the fuel cell power from total power demand via the power bus block. The default thermal system of the fuel cell model (initialised by ADVISOR) is modified by incorporating the thermal model described through Equation 4, Equation 5, Equation 6. Table 5 shows the parameters of components of the SUV used in the simulation. The coefficients of mass flow rate of hydrogen (Equation 3) and heat transfer coefficient in the radiator (Equation 5) are obtained by using the lookup table data available from ADVISOR and the curve fitting method. The derived coefficients are then shown in Table 6.

The simulations are then carried out with a sampling period (T) of 1s, the initial SoC as 0.6, and the ambient temperature at 20 °C. The EMS evaluation is conducted on two different trips - trip-1 and trip-2. Trip-1 is based on two consecutive occurrences of UDDS cycle with a top speed of 25.35 m/s and maximum acceleration and deceleration of 1.48 m/s^2 and −1.48 m/s^2 respectively whereas, trip-2 is based on two consecutive occurrences of LA92 cycle with a top speed of 30.04 m/s and maximum acceleration and deceleration of 3.08 m/s^2 and −3.93 m/s^2 respectively [53]. To examine the fuel cell degradation in each trip, the fuel cell state of health is assumed to be 100 % at the start of the journey. The total energy supplied to the vehicle is defined as

$$E_{veh} = \int \dot{m}_{H_2} LHV dt - \Delta soc V_{oc\_mean} C_{Ah\_nom} n_p n_s \quad (41)$$

Here, the first term corresponds to the total chemical energy given to the fuel cell while the second term is the total electrical energy taken out from the battery, represented by the difference between the battery energy levels at the beginning and at the end of the trip. To understand the thermal conditions of the power sources, the mean deviation of fuel cell and battery temperatures from their reference temperature is calculated. This mean value is calculated from the first time the fuel cell, battery exceeded its respective reference temperatures.

Table 6: Coefficients of Fuel Cell equations

Equations	Coefficients
$\dot{m}_{H_2}$	$\alpha_1 = 3.19 \times 10^{-15}$
	$\alpha_2 = -1.27 \times 10^{-10}$
	$\alpha_3 = 1.45 \times 10^{-5}$,$\alpha_4 = 0.016$
h_{rad}	$\beta_1 = -5.27$,$\beta_2 = 112.08$
	$\beta_3 = 134.93$
v_{htx}	$\gamma_1 = 4.07$,$\gamma_2 = -1.56$
	$\gamma_3 = 0.15$

4.2. Setting of comparative energy management strategies

The system parameters and the constraints used for all the three EMSs are the same and provided in Table 7 and Table 8 respectively. Δsoc_{cutoff} is the difference between the SoC at which the fuel cell is turned off and

Table 5: Configuration of Fuel Cell Hybrid Electric Vehicle from ADVISOR

Component	Specification	Component	Specification
Vehicle	Total mass (m_v)- 1843 kg	Fuel cell	Mass of fuel cell (m_{fc}) - 125 kg
	$c_{rolling}$ - 0.009		Heat capacity of fuel cell (Cp_{fc}) - 500 J/kgK
	Gear ratio (gr) - 10.549		Cabin heating efficiency (η_{cabin}) - 0.7
	Accessory ($P_{accessory}$) - 700 W		Mass flow rate of air in cabin $\dot{m}_{cabin}$ - 0.07 kg/s
	Transmission - one speed	Battery	Nominal capacity(C_{Ah_nom}) - 6Ah
Motor	Type - Induction motor		No. of series connection (n_s)- 27
	Maximum power - 107 kW		No. of parallel connection (n_p) - 2
	Peak efficiency - 0.94		Eff. thermal resistance - on (R_{on}) - 1.12 W/K
Fuel cell	Max. power - 55 kW		Eff. thermal resistance - off (R_{off}) - 7.81 W/K
	Peak efficiency (η_{max}) - 0.55		Heat capacity of module (Cp_{module}) - 795 J/kgK
	LHV of H_2 - 120 000 J/g		Mass of module (m_{module}) - 1.1347 kg
	Time constant (t_s) - 1.5 s		Mass flow rate across module ($\dot{m}_{air}$)- 0.0058 kg/s
	Frontal area of radiator (A_{rad}) - 0.2 m^2		

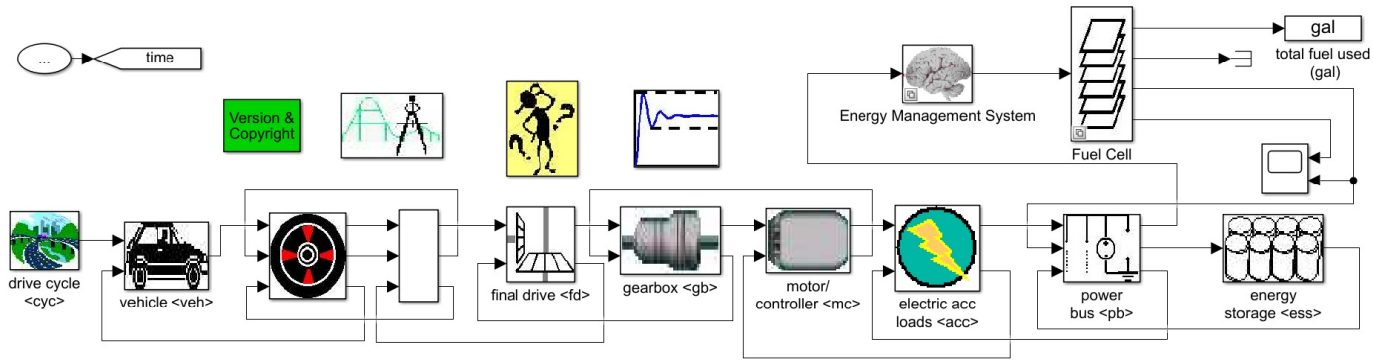

Figure 6: Simulink design of SUV FCHEV model integrated comparative EMSs

Table 7: Parameters of EMSs used in the simulation.

Parameter	Value
Δsoc_{cutoff}	0.05
soc_{nom}	0.6
P_{b_max}	75 kW
$\dot{m}_{H_2 max}$	0.8208 g/s
$u_{working\_min}$	2500 W
θ_{FCM}	-1.2
$w_{degrade}$	1000
$w_{terminal}$	2
$t_{fc\_min\_off}$	90 s
$t_{fc\_min\_on}$	60 s
T_{fc_cutoff}	70 °C
T_{fc_ref}	60 °C
T_{b_cutoff}	35 °C
T_{b_ref}	33 °C
$V_{maxdrop}$	0.2 V

Table 8: Upper and lower limits of operating variables

Variable	Minimum	Maximum
P_{fc}	0 W	50 000 W
$\dot{P}_{fc}$	−3000 W/s	3000 W/s
T_{fc}	20 °C	80 °C
soc	0.4	0.8
V_b	162 V	315.9 V
T_b	20 °C	50 °C

the nominal value of SoC. This parameter is used as the final measure to prevent overcharging of the battery by turning off the fuel cell and running the vehicle in pure battery mode. The control and prediction horizons are both set to N=4. Due to the number of variables and cost components involved in the optimization process, the small prediction horizon is selected to reduce the computational effort. The control horizon is taken to be the same as the prediction horizon to provide freedom to the optimizer to properly choose control commands at each step.

While the AMPC is constructed as presented in Section 3, the MPC-1 has a simplistic cost function with $C_{stage}(k) = C_{m_{H_2}} + C_{P\_batt} + C_{soc}$ and no terminal cost. Meanwhile, the MPC-2 uses the proposed cost function (Equation 21 - Equation 27) with constant weights. Table 9 shows the weight selection for the cost components of the MPC-1 and MPC-2. For the MPC-1 and MPC-2, these weight values are calibrated for trip-1 and then re-used for trip 2. The weights of cost function for the AMPC are automatically regulated online by the FCM (see Subsection 3.4).

Table 9: Weights of cost components for MPC-1 and MPC-2 during simulation

Weight	MPC-1	MPC-2
W_1	1	1
W_2	0.333	0.2737
W_3	0	0.5826
W_4	0	1.2
W_5	1.3333	1.8
W_6	0	0.7227
W_7	0	1.5

4.3. Results and discussions

The comparative simulation results and the AMPC weight profile according to trip-1 are shown in Figure 7, Figure 8 and Figure 9. The same for trip-2 are then shown in Figure 10, Figure 11 and Figure 12. The upper and lower limits, reference values and cut-off values set for the fuel cell and battery can be seen in Figure 7, Figure 8, Figure 10 and Figure 11. The performance of EMSs for trip-1 and trip-2 are discussed in the upcoming sections.

4.3.1. Comparison of EMSs performance in trip-1

In trip-1, the three EMSs met the total power demand to the energy sources, as seen in the total power plot

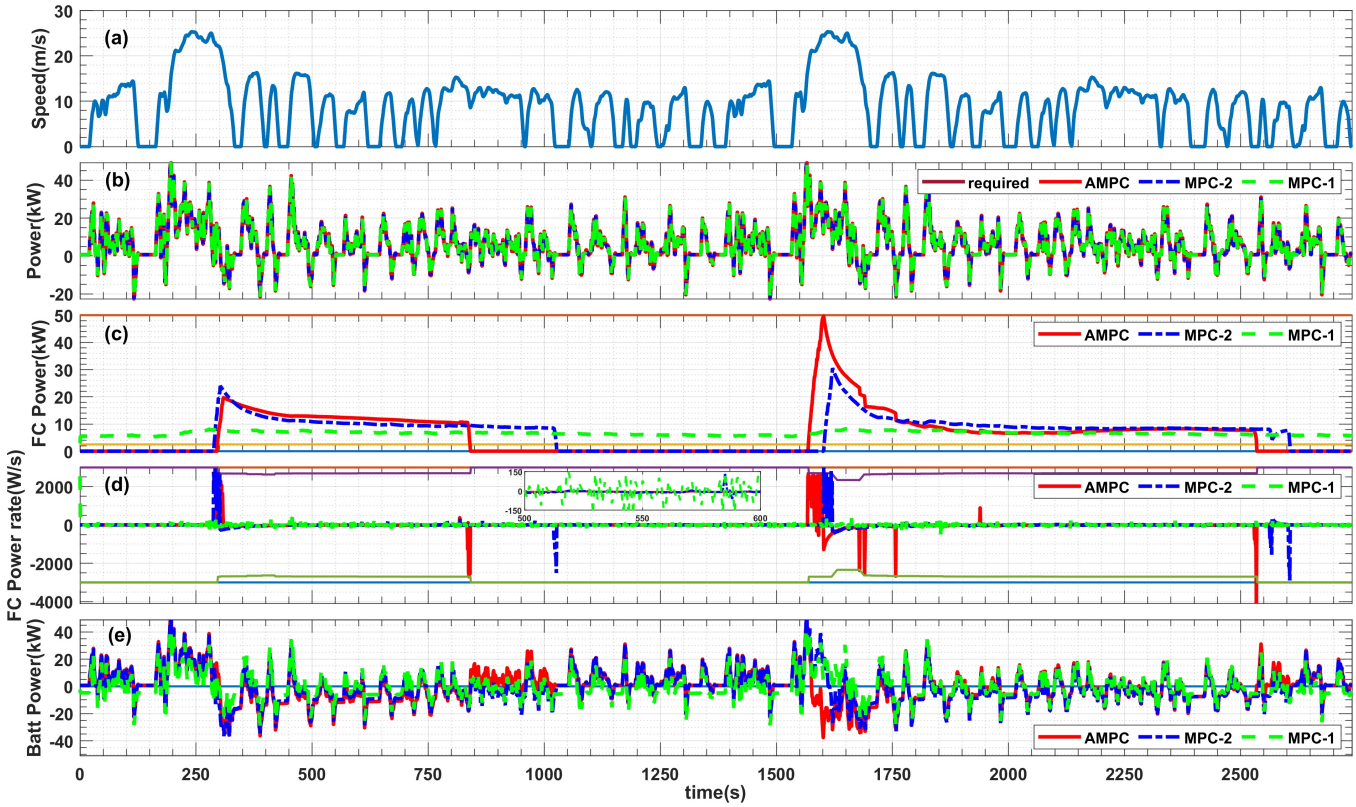

Figure 7: Trip 1 simulation result - a) Vehicle speed, b) Total power requested and provided by EMSs, Comparison of c) Fuel cell power, d) Fuel cell power rate and e) Battery power under different EMSs

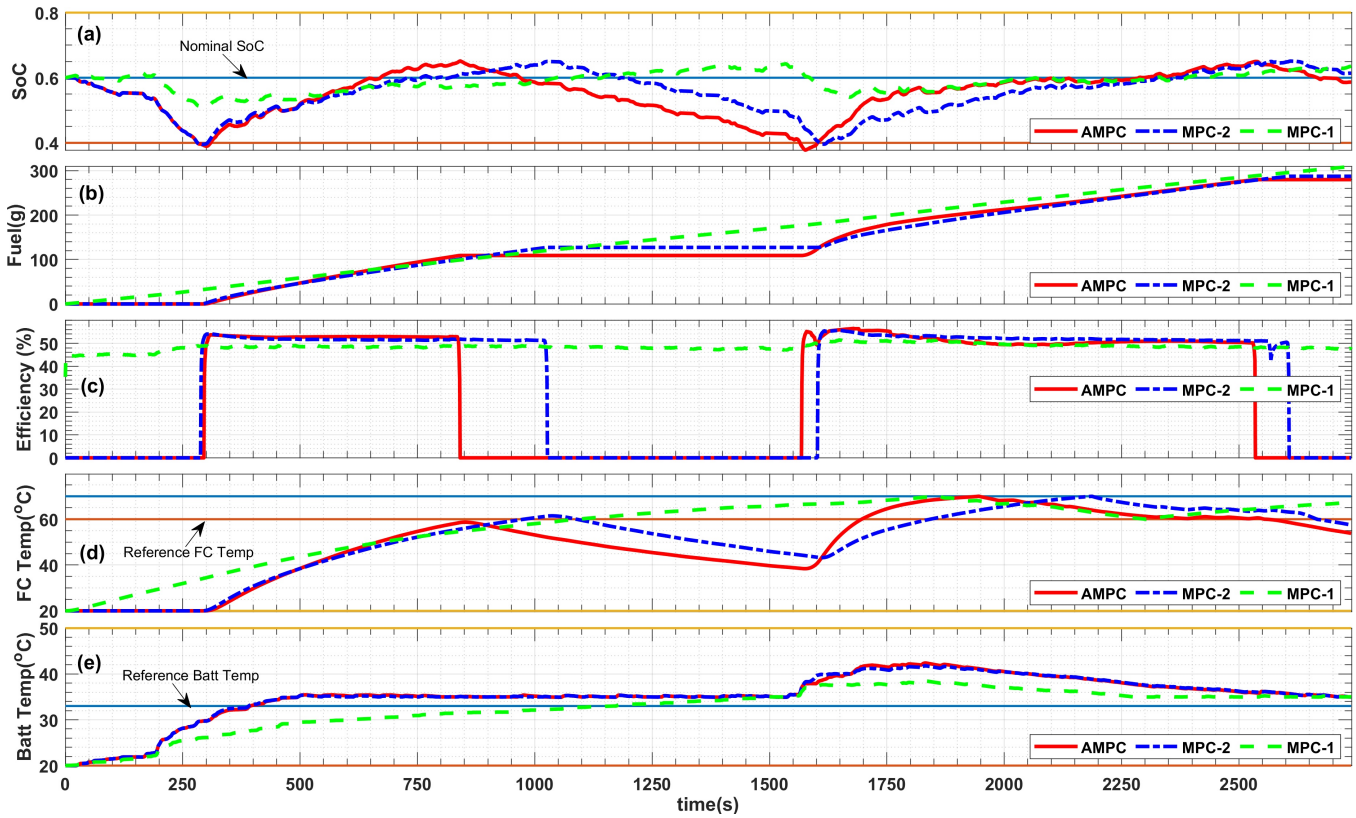

Figure 8: Trip 1 simulation result - Comparison of a) State of Charge of battery, b) Fuel consumed, c) Efficiency of fuel cell, d) Fuel cell temperature and e) Battery temperature under different EMSs

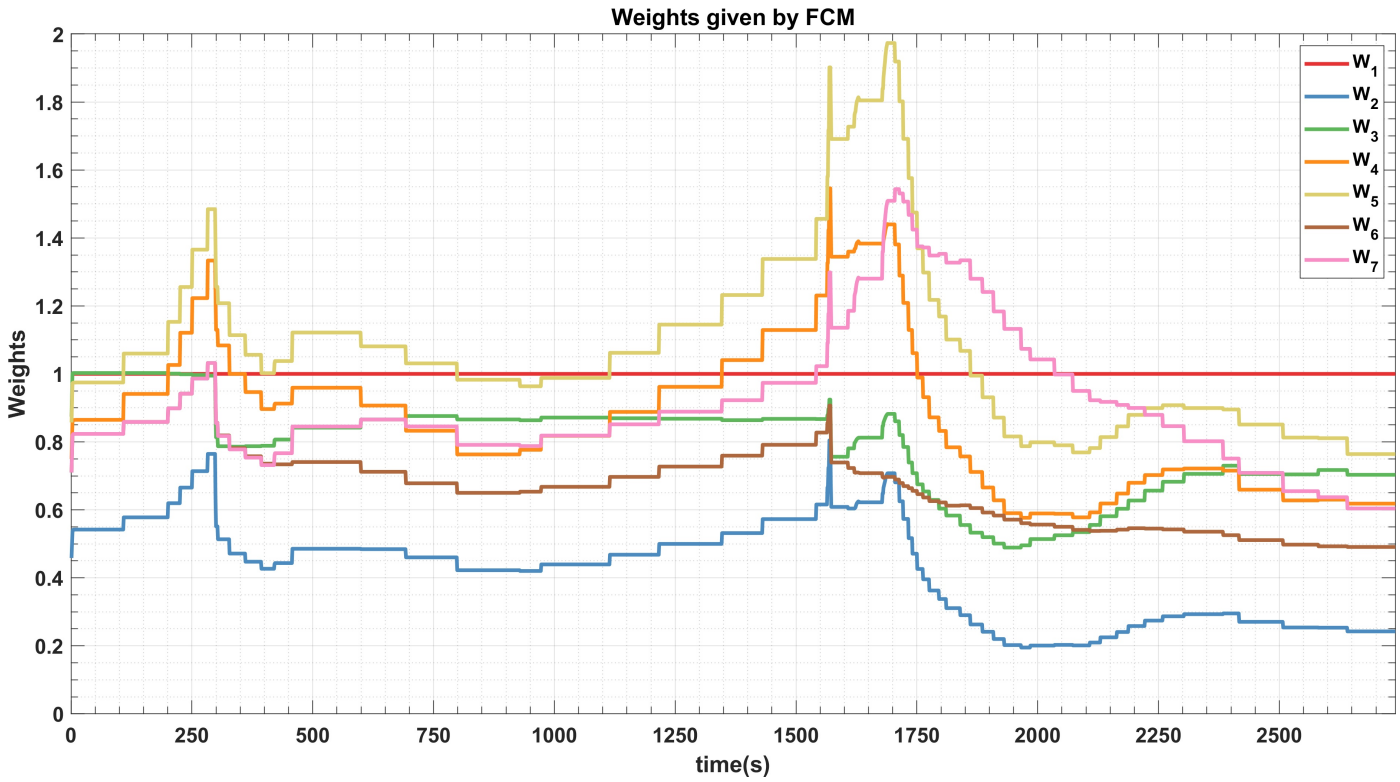

Figure 9: Trip 1 simulation result: AMPC weights regulated by FCM

Figure 7b. The performance of the MPC-1 in trip-1 is first analyzed. As seen in Figure 8a,d,e, the SoC of the battery is kept near the initial value throughout trip-1, and the fuel cell and battery temperatures gradually increase. It is due to the fact that the fuel cell's average power of 6.57 kW (Figure 7c) provides nearly continuous power while the average power demand of trip-1 is 6.22 kW. As a result, the net battery power is low, resulting in a low SoC deviation and a moderate battery temperature rise. However, due to the fuel cell's continuous low-power operation in trip-1, the temperature of the fuel cell has increased (Figure 8d), the efficiency has reduced (Figure 8c), and the fuel consumption has increased (Figure 8b). In the case of MPC-1, high-frequency oscillation is observed in the system response, as shown in a zoom-in of Figure 7d. The MPC-1's poor performance could be related to using a small number of cost components that do not account for fuel cell efficiency, operating temperature, or deterioration and instead focus on fuel consumption and battery power.

As observed in Figure 7c,e, the second EMS, MPC-2, used the battery significantly in trip-1, reducing the reliance on fuel cell. The SoC of the battery fluctuated from minimum to the SoC cutoff value (Δsoc_{cutoff}), at which point the fuel cell is switched off. The battery temperature increased as a result of increased usage. The surges in battery temperatures at t = 200 s and 1550 s (Figure 8e) are caused by surges in battery power provided to the vehicle (Figure 7e). All of these trends are caused by the on/off supply of fuel cell power. When the power demand is high and the fuel cell is off, the battery has to provide a large amount of power as seen in times t = 200 s and 1550 s. The on/off supply of fuel cell power also had impact on the fuel cell performance as well. Throughout the journey, it was observed that the fuel cell temperature has increased and decreased unlike the case of the MPC-1. When the fuel cell is off, the cooling system can effectively cool the fuel cell due to the lack of heat generation. A drop of 20 °C is observed between time t = 850 s and t = 1600 s (Figure 8d). The MPC-2 has operated the fuel cell in the best efficient region as seen in Figure 8b. Subsequently, it has helped in minimising the fuel consumption (see Figure 8). The power transient during fuel cell operation is considerably reduced when compared to the MPC-1. The enhanced performance of MPC-2 compared to MPC-1 can be attributed to the cost function formulation, which includes various objectives for the fuel cell's ($C_{fc\_rate}, C_{fc\_eff}, C_{T\_fc}$) and battery's ($C_{T\_b}$) welfare are provided. The design of C_{fc_eff} discourages switching on and favours switching off of the fuel cell, which aids the optimizer in determining when to turn on/off the fuel cell as needed.

The proposed EMS, AMPC, operated similarly to MPC-2, but the AMPC provided more fuel cell power and thus could support the battery. This is evidenced by the rapid increase in SoC at times t = 650 - 850 s and t

= 1600 - 1700 s in Figure 8a. By operating in a higher power region, the fuel cell charges the battery faster and shuts down earlier than the MPC-2. The duration of fuel cell off has increased by 23% in the case of AMPC compared to MPC-2 while meeting power demand, as shown in Figure 7c. As seen in Table 10, this allowed for further reductions in fuel cell temperature as well as a shorter duration of low power fuel cell operation.

The AMPC uses the dynamic weights obtained from FCM to compute the optimal control decision. The output concepts $W_1 - W_7$, and the factors W_8 and W_9, influence the optimizer's decisions by modifying the weights of the cost function and the domain of the control variable (fuel cell power), respectively in order to enhance the performance of NMPC in the AMPC architecture. The magnitude and distribution of the weights in Figure 9 show that the priority and significance of the priority vary.

The weights $W_1 - W_7$ are normalized by dividing by weight W_1 as shown in Figure 9. From the start of the journey until t = 300 s, the SoC dropped to a minimum value, and in response to the drop, the weights W_2, W_4, W_5 grew while the weights W_1, W_3 decreased, as designed in column A_1 of Table 3. The fuel cell efficiency (W_4) was given more importance than fuel consumption (W_1) and transients (W_3), encouraging the fuel cell to perform more efficiently and supply power for both traction and charging the battery. The weights W_6, W_7 are increased compared to W_1, in reality, they remained constant as there was no input concept activation for W_6, W_7 between t = 0 and 300 s. At t = 300 s, when the fuel cell was turned on, the input concept A_8 was activated. The fuel cell power transients during start-up activated the input concept A_5. The activation of concept A_5, A_8 increased weight W_1 and reduced all other weights relative to W_1, creating a sudden drop in weights. The weights W_2, W_4, W_5, W_7 dropped relative to W_1 when SoC grew from t = 300 s due to charging till t = 400 s. At t = 400 s, the input concept A_3 related to battery temperature was triggered as the temperature crossed the reference value. The weights increased slightly as the battery temperature increased slowly. Between time t = 400 – 950 s, the SoC reached the nominal value and crossed it, while the temperature stayed constant. As a result, W_1 has increased further, and all other weights have decreased and below W_1, demonstrating that once the battery's SoC is sufficient to match the vehicle's demand, reducing fuel consumption becomes a higher priority. From t = 950 to 1550 s, the weights W_2, W_4, W_5, W_7 grew at a large rate, while W_6 increased at a smaller rate in response to diminishing SoC and reaches a peak. When the fuel cell turns on the second time at t = 1550 s, it caused a drop in weights for the reasons stated above. Between t = 1550 and 1700 s, the battery temperature reached a new peak, prompting the FCM to increase the weights. At time t = 1700 s, the concept A_2 was activated as the fuel cell temperature crossed the reference value. The activation of A_2 increased weights W_1, W_6, W_7 and decreased weights W_2, W_3, W_4, W_5, allowing the fuel cell to operate at lower power for the battery to take over, as designed in the column A_2 in Table 3. The highest drop was observed in weights W_2, W_3, W_4, W_5, when the causal weights are of opposite signs. During the period t = 2000 - 2250 s, when both fuel cell and battery temperatures were decreasing, the weights stabilised and began to reverse trend, and from t = 2250 s, since the SoC was near to the nominal value, the weights are adopted such that the function of the fuel cell is reduced and that of the battery is increased.

Depending on the fuel cell transient, the factors W_8, W_9 reduce the rate of change of the fuel cell power limit. When the fuel cell is turned off, the transients are zero, hence the limits remain unchanged. However, when the fuel cell is turned on or off, there is a large transient in fuel cell power, and the limits of fuel cell power transients are reduced as seen in Figure 7d. If no transients exist in the fuel cell power during operation, the factors are not updated, and the limits remain unchanged. Otherwise, if there have been transients in the past one minute, the factors are updated, further lowering the limits, as seen in Figure 7d near the time t = 1650 s.

4.3.2. Comparison of EMSs performance in trip-2

The trip-2 is used to study the performance of EMS in previously unseen harsher accelerations and decelerations as all three EMSs are tuned for trip-1. Trip-1 has less power demand than trip-2 due to lower accelerations and decelerations and shorter peak velocity durations, as shown in Figure 7a, b and Figure 10a, b. In trip-2, from the total power plot Figure 10b, it can be observed there are some deviation in braking power required and braking power provided by all three EMSs. It is because the braking power is more than the battery's capacity to absorb the regenerative power and the capacity of mechanical brakes, resulting in a slight deviation in velocity achieved and requested (Table 10). One observation regarding the battery temperatures in trip-2 is that they are larger than in trip-1 for all three EMSs. It is due to the trip-2's consistent high power demand. When a sudden peak vehicle power demand arises, the fuel cell may not be able to scale the power to the required value due to constrains in rate of change of power. In such cases, the battery power requirement may reach the limits of the battery. The power required is high in trip-2 near the time instances t = 300 s, 850 s (Figure 10b), and the fuel cell was unable to provide the required power (Figure 10c), so the battery power reached its maximum limit, and the battery temperature also took a large jump, as shown in the battery power and battery temperature plots in Figure 10e and Figure 11e respectively.

At the start of trip-2, the MPC-1 was focused on limiting fuel consumption and battery usage. It can be

Figure 10: Trip 2 simulation result - a) Vehicle speed, b) Total power requested and provided by EMSs, Comparison of c) Fuel cell power, d) Fuel cell power rate and e) Battery power under different EMSs

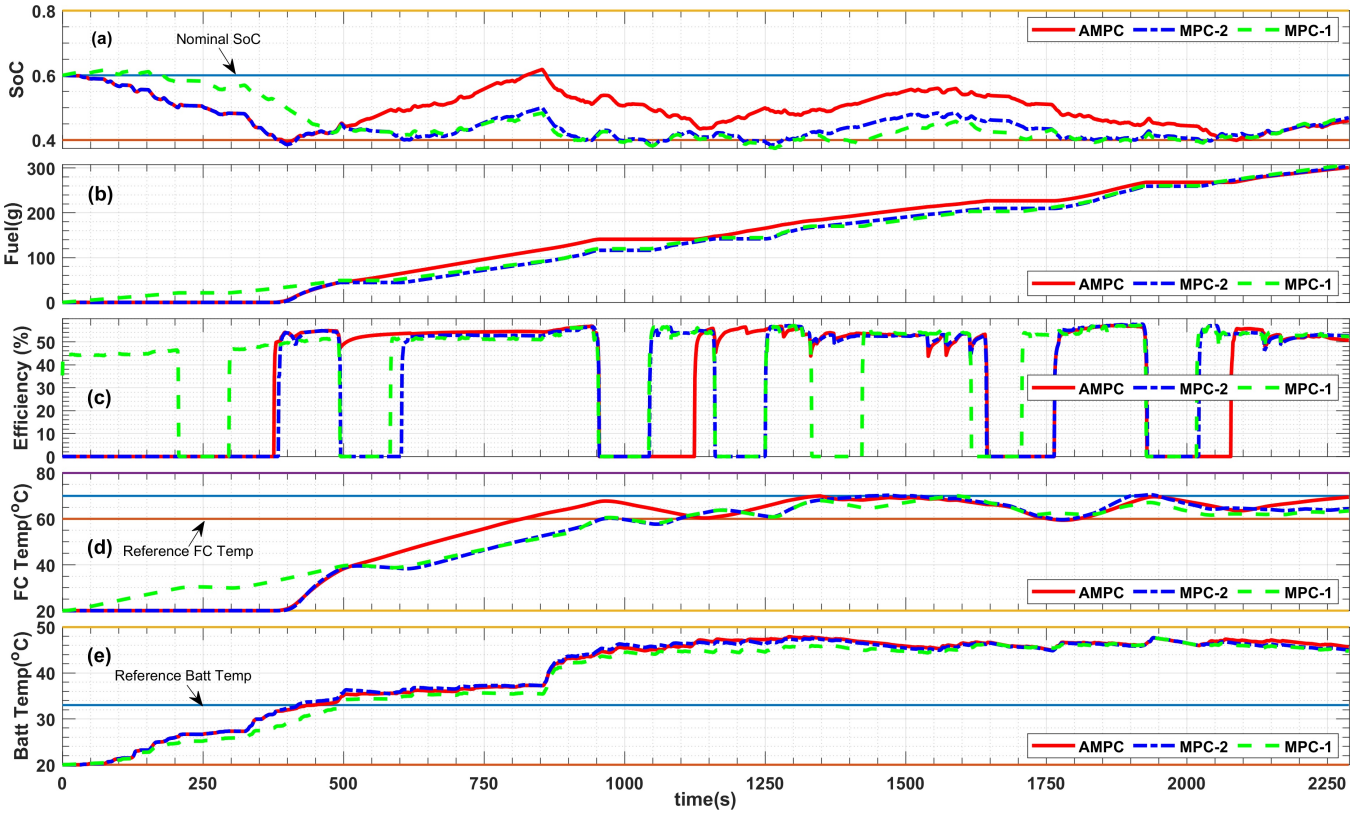

Figure 11: Trip 2 simulation result - Comparison of a) State of Charge of battery, b) Fuel consumed, c) Efficiency of fuel cell, d) Fuel cell temperature and e) Battery temperature under different EMSs

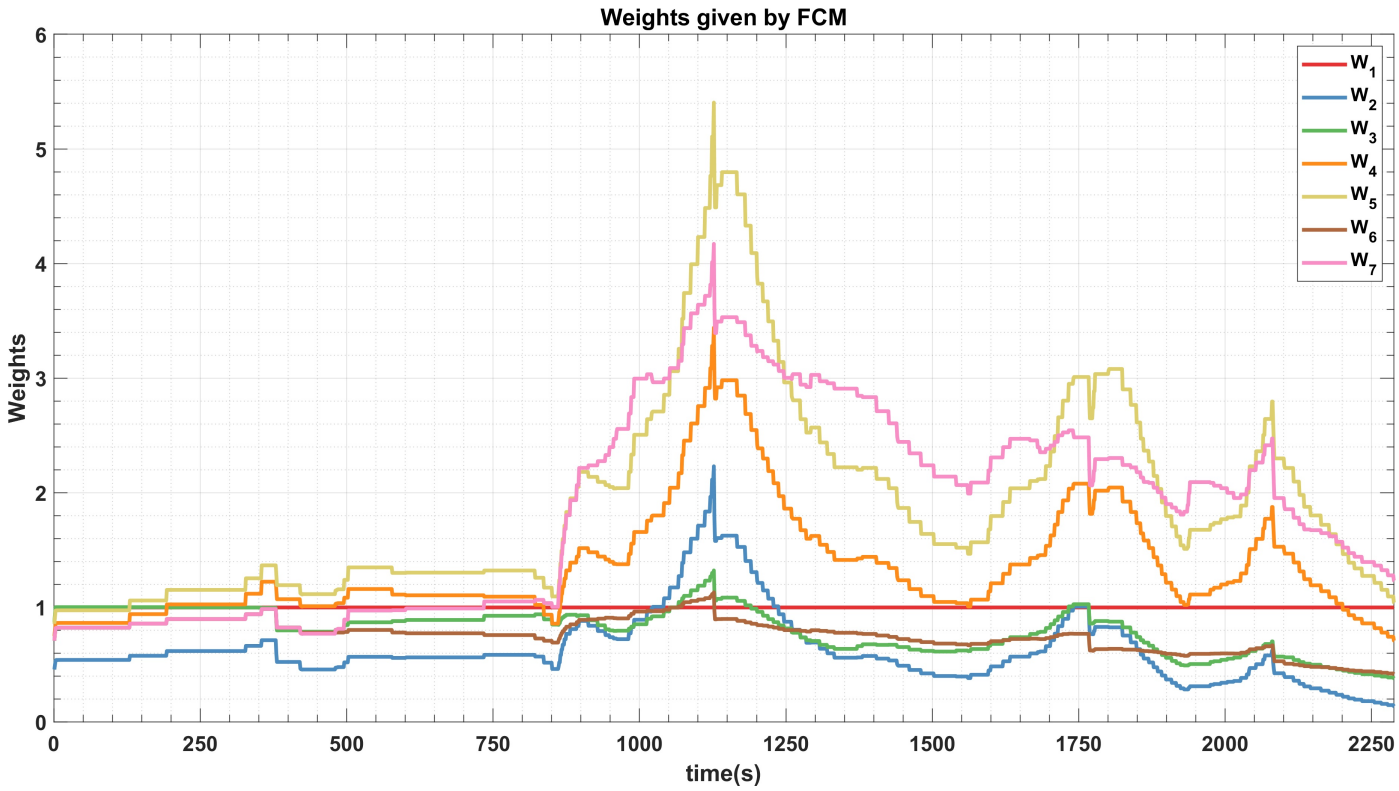

Figure 12: Trip 2 simulation result: AMPC weights regulated by FCM

inferred from the low power operation of the fuel cell (Figure 10c) and lower battery power (Figure 10e) from the start of the trip until time t = 350 s. When the SoC dropped to a minimum at time t = 600 s, the fuel cell tried to enhance the battery SoC (Figure 11a), as evidenced by the rapid increase in fuel cell power in the Figure 10c. Minimizing battery power resulted in lower battery temperatures at first, but by t = 1500 s, all three EMSs had the same battery temperatures. This can be explained by the MPC-1's increased battery usage, as considerable variations in SoC can be seen near time t = 1500 s. As indicated in the total power and fuel cell power plot in Figure 10, the MPC-1 frequently turned off the fuel cell as the vehicle decelerated. This resulted in large transients in fuel cell power, as shown in the Figure 10d. It should be noticed that the duration of each fuel cell switch off is 90 s, which is the minimum switch off duration Δt_{off}. Except at t = 200 s, the fuel cell was turned on to charge the battery and provide the required traction. At t = 200 s, the fuel cell was turned on to reduce battery power until t = 350 s. The rise in fuel cell temperature is limited by low power output and frequent switch off (Figure 10d). Nonetheless, in trip-2, the increased frequency of start/stop events and strong transients in fuel cell power (Figure 10d) are the primary reason for the fuel cell's poor health, with a SoH drop of 0.12% by the end of the trip.

In the instance of MPC-2, it can be seen from the SoC plot Figure 11a and the fuel cell power plot Figure 10c that the SoC of the battery and the response of the fuel cell are comparable to the MPC-1 after t = 500 s, however, the number of on/off operation and transients during operation of fuel cell is smaller. Because the fuel cell power output is similar to MPC-1, the fuel cell temperature after t = 500 s is likewise similar. The MPC-2 and MPC-1 responses are comparable because, after switching off the fuel cell at t = 500 s due to braking, the SoC in both the EMSs declined from 0.45 at t = 500 s to 0.4 at t = 600 s (Figure 11a). Since the EMS must maintain SoC while simultaneously taking into account the aims and constraints of power sources, the response of the EMSs, i.e., fuel cell power, is similar but differs depending on the objectives of each EMS. One of the goals of MPC-1 is to reduce fuel consumption and hence lower power production, while MPC-2's goal is to run the fuel cell at higher efficiency with less transients. These varied EMS objectives yield diverse responses, which can be seen in the fuel cell power (Figure 10c), power transient (Figure 10d), and efficiency plots (Figure 11c) for example, from t = 600 s to t = 950 s. The transients during switch off are high due to the sudden availability of braking power at times t = 500, 950, 1150, 1650, and 1950 s, while the transients during start-up are high at times t = 375, 1050, 1250, and 2000 s. The fuel cell is switched on faster to provide traction and charge the battery faster as SoC is low in those instances. Transients during operation are also observed between t = 1750 -

1950 s (Figure 10d).

The AMPC maintained the SoC near to the nominal value better than MPC-1 and MPC-2 (Figure 11a). The AMPC achieved this by a) careful computation of fuel cell switch off instant and duration; b) operating the fuel cell at higher efficiency (Figure 11). We can see that in some instances (near the times t = 500 s and t = 1150 s) where there are large decelerations, the fuel cell was shut down by the MPC-1 and MPC-2 due to high regenerative braking power from the motor, whereas instead of switching off, the AMPC reduced the fuel cell power, as seen in Figure 10c. The AMPC sent the energy from fuel cell to the battery, resulting in less capacity to accommodate the regenerative energy. Nonetheless, there are two benefits to doing this: a) reducing the number of switching to improve the fuel cell lifespan; b) in the event of a sudden massive acceleration after the deceleration, as seen in these instances, the fuel cell supplies power, to reduce the load on the battery and hence improve its lifetime, as opposed to the MPC-1 and MPC-2. In trip-2, compared to the MPC-1 and MPC-2, the lowest number of fuel cell on/off operations was achieved by AMPC (Table 10). The AMPC had lower transients during fuel cell start-up than MPC-1 and MPC-2 because, the battery's SoC is sufficient to provide power until the fuel cell power can increase at a moderate rate. Because of the high power generation in the fuel cell and the low number of switch offs, the fuel cell temperature rose quickly in time t = 500 - 950 s (Figure 11d). Nonetheless, the fuel cell temperature becomes comparable to other EMSs fuel cell temperatures due to radiator cooling in the fuel cell.

Figure 12 shows the weights regulated by the fuzzy cognitive map in the AMPC for trip-2. Due to increased battery temperature in trip-2, the weights $W_2 - W_7$ are 1.5 times larger than trip-1 with weight W_1 normalized to 1.

The trend observed in Figure 9 at the start of trip-1, during minimum SoC, start-up of fuel cell, and activation of concept A_3, is also exhibited at the start of trip-2 and at times t = 300 s, t = 350 s, and t = 425 s respectively (Figure 12). As the battery temperature grew gradually owing to charging between times t = 500 - 850 s, the weight W_7 climbed while the weight W_6 declined, as determined from causal weights in column A_3 of Table 3. As the SoC reached nominal value, the weights declined from t = 800 - 850 s, and the concept A_2 was activated at time t = 825 s. Due to a significant rise in battery temperature due to huge battery power, the weights $W_2, W_4 W_5, W_6, W_7$ increased whereas W_1, W_3 decreased at t = 850 s. Weights $W_2, W_4, W5$ drop as fuel cell temperature increased, whereas W_6 increased till t = 900 s. Weights increased from t = 950 s to t = 1125 s due to the increased battery temperature and reduced SoC. The weight decreased when the fuel cell was turned on for the second time for the reasons explained in the case of fuel cell start-up in trip-1. The weights decreased in the intervals t = 1125 -1550 s, t = 1775 – 1950, and t = 2075 s – until the end of trip -2 as the fuel cell temperature rose, whereas the weights increased in the intervals t = 1550 – 1775 s and t = 1950 – 2075 s as the fuel cell temperature decreased and SoC deviated from the nominal value. It is observed that the magnitude of the weights decreases at each peak. It is due to the degradation concept associated with fuel cell start/stop cycles A_8, which causes the weight W_1 to grow as the number of start/stop cycles increases. This is done to give fuel consumption greater importance and limit the number of switching on when the fuel cell is off. Due to the logic employed in the FCM, the SoC was well maintained near nominal value in trip-2 with fewer fuel cell switch on/off cycles.

4.3.3. Overall performance of EMSs

The simulation results of all three EMS are summarized in the Table 10. In the case of AMPC, the average improvement in hydrogen consumption in the two journeys

Table 10: Comparison of numerical results of MPC-1, MPC-2 and AMPC

Parameters	Trip-1			Trip-2		
	MPC-1	MPC-2	AMPC	MPC-1	MPC-2	AMPC
RMS Error in velocity (m/s)	0	0	0	0.0046	0.0046	0.0046
Total Fuel Consumed (g)	309.27	287.22	279.73	307.03	303.75	300.78
Total Energy given to the vehicle (MJ)	36.57	34.26	33.77	38.80	38.47	38.25
Final SoC-Initial SoC	0.0354	0.0137	-0.0135	-0.1275	-0.1313	-0.1406
Average Efficiency (%)	48.43	51.95	51.91	51.76	53.25	53.44
State of health of Fuel Cell (%)	99.98	99.97	99.97	99.88	99.91	99.94
Mean deviation from $T_{fcref}(^0C)$	4.95	-1.23	-3.84	3.83	4.90	5.65
Mean deviation from $T_{bref}(^0C)$	2.75	3.81	3.85	10.14	10.68	10.90
Low Power Duration (s)	2739	1132	755	666	483	480
High Power Duration (s)	0	0	19	3	12	2
Number of Start/Stops	1	2	2	8	6	4

compared to MPC-1 and MPC-2 was 6.131% and 1.865%, respectively. Due to the increased power requirement in trip-2, the total energy amounts provided to the vehicle in the three cases are similar. If the driving conditions of trip2 are extrapolated for 100 hours, the improvement in SoH of fuel cell in the case of AMPC compared to MPC-1 and MPC-2 is 11.7% and 5.5% respectively. Because the fuel cell is the most expensive component in the car, improving its SoH is beneficial for extracting utility over a longer period of time. The drop in mean deviation of fuel cell temperature for the MPC-1 and MPC-2 compared to AMPC is due to the high frequency of fuel cell turn off. This is offset by the higher SoH of the fuel cell under AMPC strategy. For trip-1, the drop of 8.8 °C in fuel cell temperature in AMPC compared to MPC-1 is significant because a lower operating temperature of a fuel cell can minimize thermal stress and hence work for a longer period of time. In both the trips, the fuel cell life is extended compared to the other two EMS by minimizing the depletion of SoH of fuel cell and minimizing the fuel cell temperature.

5. Conclusion and future work

In this paper, an Advanced Model Predictive Control is proposed for optimal energy management in FCHEVs. The AMPC employs a novel dynamic multi-objective cost function that considers fuel consumption, operational efficiency, fuel cell health, battery state of charge, and lastly fuel cell and battery temperatures in order to prolong the lifetime of components and lower the overall running cost of FCHEV. A Fuzzy Cognitive Map is constructed for AMPC to continuously regulate the cost function weights to optimise the energy management performance. The proposed controller has been compared with two conventional constant weighted NMPC based EMSs by numerical simulation. The simulation results show that the AMPC offers the best performance by reducing fuel consumption, total energy given to the vehicle, and improving the lifetime of fuel cells by controlling the number of fuel cell on/off, efficient operation and lower fuel cell operating temperature compared to MPC-1 and MPC-2. It is due to the adaptive nature of dynamic weights of NMPC regulated by the FCM. Another key benefit of AMPC is that it requires little effort for calibrating the EMS due to the generalized and easily comprehensible causality between the states of the vehicle (input concepts) and NMPC cost function weights (output concepts) enabled by the proposed FCM architecture.

Future work will be carried out with an updation of causality weight matrix of FCM using artificial intelligence - based learning techniques to improve the adaptability as well as robustness of the AMPC. In another research direction, the auxiliary power in the fuel cell and battery system will be analysed for inclusion in the AMPC.

Appendix A. Battery Equations

Equations of Coulombic Efficiency C_{eff} and Maximum Capacity of the battery C_{Ah} ,Open circuit Voltage V_{oc}, Charging resistance r_{chg}, Discharging resistance r_{dis} are obtained by fitting the battery lookup table data available in ADVISOR.

$$C_{eff} = \delta_1 T_b^2 + \delta_2 T_b + \delta_3 \tag{A.1}$$

$$C_{Ah} = \zeta_1 T_b^2 + \zeta_2 T_b + \zeta_3 \tag{A.2}$$

$$\begin{aligned} V_{oc} = {} & \alpha_1 + \alpha_2 T_b + \alpha_3 soc + \alpha_4 T_b^2 + \alpha_5 T_b soc + \alpha_6 soc^2 + \\ & \alpha_7 T_b^2 soc + \alpha_8 T_b soc^2 + \alpha_9 soc^3 + \alpha_{10} T_b^2 soc^2 + \alpha_{11} T_b soc^3 \\ & + \alpha_{12} soc^4 + \alpha_{13} soc^5 + \alpha_{14} soc^4 T_b + \alpha_{15} soc^3 T_b^2 \end{aligned} \tag{A.3}$$

$$\begin{aligned} r_{chg} = {} & \beta_1 + \beta_2 T_b + \beta_3 soc + \beta_4 T_b^2 + \beta_5 T_b soc + \beta_6 soc^2 + \\ & \beta_7 T_b^2 soc + \beta_8 T_b soc^2 + \beta_9 soc^3 + \beta_{10} T_b^2 soc^2 + \beta_{11} T_b soc^3 \\ & + \beta_{12} soc^4 + \beta_{13} T_b^2 soc^3 + \beta_{14} T_b soc^4 + \beta_{15} soc^5 \end{aligned} \tag{A.4}$$

$$\begin{aligned} r_{dis} = {} & \gamma_1 + \gamma_2 T_b + \gamma_3 soc + \gamma_4 T_b^2 + \gamma_5 T_b soc + \gamma_6 soc^2 + \\ & \gamma_7 T_b^2 soc + \gamma_8 T_b soc^2 + \gamma_9 soc^3 + \gamma_{10} T_b^2 soc^2 + \gamma_{11} T_b soc^3 \\ & + \gamma_{12} soc^4 + \gamma_{13} T_b^2 soc^3 + \gamma_{14} T_b soc^4 + \gamma_{15} soc^5 \end{aligned} \tag{A.5}$$

Table Appendix A.1: Coefficients of equations for battery

Eqs	Coefficients
V_{oc}	$\alpha_1 = 10.31$,$\alpha_2 = -0.05814$,$\alpha_3 = 2.043$
	$\alpha_4 = 0.0008699$,$\alpha_5 = 0.3595$,$\alpha_6 = -9.587$
	$\alpha_7 = -0.004332$,$\alpha_8 = -0.8736$,$\alpha_9 = 26.31$
	$\alpha_{10} = 0.007505$, $\alpha_{11} = 0.8867$, $\alpha_{12} = -28.31$
	$\alpha_{13} = 10.93$,$\alpha_{14} = -0.3132$,$\alpha_{15} = -0.004072$
r_{chg}	$\beta_1 = 0.06283$,$\beta_2 = -0.001489$,$\beta_3 = -0.128$
	$\beta_4 = 1.77 \times 10^{-5}$,$\beta_5 = -0.00924$,$\beta_6 = 0.6212$
	$\beta_7 = 0.0002199$,$\beta_8 = 0.02236$, $\beta_9 = -1.571$
	$\beta_{10} = -0.0005006$, $\beta_{11} = -0.01379$, $\beta_{12} = 1.712$
	$\beta_{13} = 0.0002911$,$\beta_{14} = 0.0003481$,$\beta_{15} = -0.6516$
r_{dis}	$\gamma_1 = 0.1311$,$\gamma_2 = 0.006381$,$\gamma_3 = -0.8978$
	$\gamma_4 = -0.0001372$,$\gamma_5 = -0.07916$,$\gamma_6 = 4.631$
	$\gamma_7 = 0.00135$,$\gamma_8 = 0.2015$,$\gamma_9 = -11.3$
	$\gamma_{10} = -0.002685$, $\gamma_{11} = -0.1869$, $\gamma_{12} = 12.24$
	$\gamma_{13} = 0.001516$,$\gamma_{14} = 0.05568$,$\gamma_{15} = -4.749$
C_{eff}	$\delta_1 = -1.841 \times 10^{-5}$,$\delta_2 = 0.00134$, $\delta_3 = 0.968$
C_{Ah}	$\zeta_1 = -0.000727$,$\zeta_2 = 0.06563$, $\zeta_3 = 5.943$

Appendix B. Motor Equations

The maximum torque and power required by the motor are obtained by fitting the motor lookup table data available in ADVISOR.

$$T_{max} = \epsilon_1\omega_m^6 + \epsilon_2\omega_m^5 + \epsilon_3\omega_m^4 + \epsilon_4\omega_m^3 + \epsilon_5\omega_m^2 + \epsilon_6\omega_m + \epsilon_7 \tag{B.1}$$

$$P_{motor} = \rho_1 + \rho_2\omega_m + \rho_3\omega_m^2 + \rho_4\omega_m T_m + \rho_5 T_m^2 + \rho_6\omega_m T_m^2 + \rho_7\omega_m^2 T_m^2 + \rho_8 T_m^4 + \rho_9\omega_m T_m^4 \tag{B.2}$$

Table Appendix B.1: Coefficients of equations for electric motor

Eqs	Coefficients
T_{max}	$\epsilon_1 = 15.19$,$\epsilon_2 = -8.746$,$\epsilon_3 = -66.71$,$\epsilon_4 = 47.96$
	$\epsilon_5 = 78.79$,$\epsilon_6 = -124.1$,$\epsilon_7 = 155.1$
P_{motor}	$\rho_1 = 2832$,$\rho_2 = -15.03$,$\rho_3 = 0.01907$,$\rho_4 = 1$
	$\rho_5 = -0.1376$,$\rho_6 = 0.001626$,$\rho_7 = 3.204 \times 10^{-7}$
	$\rho_8 = 2.358 \times 10^{-6}$,$\rho_9 = -1.403 \times 10^{-8}$

References

[1] J. T. Pukrushpan, A. G. Stefanopoulou, H. Peng, Modeling and control for PEM fuel cell stack system, Proceedings of the American Control Conference 4 (February) (2002) 3117–3122. doi:10.1109/acc.2002.1025268.

[2] A. Arce, A. J. del Real, C. Bordons, MPC for battery/fuel cell hybrid vehicles including fuel cell dynamics and battery performance improvement, Journal of Process Control 19 (8) (2009) 1289–1304. doi:10.1016/j.jprocont.2009.03.004.

[3] L. Guzzella, A. Sciarretta, Vehicle Propulsion Systems:Introduction to Modeling and Optimization, 3rd Edition, Springer-Verlag Berlin Heidelberg, 2013. doi:10.1007/978-3-642-35913-2.

[4] P. Thounthong, S. Raël, B. Davat, Control strategy of fuel cell/supercapacitors hybrid power sources for electric vehicle, Journal of Power Sources 158 (1) (2006) 806–814. doi:10.1016/j.jpowsour.2005.09.014.

[5] A. Khajepour, S. Fallah, A. Goodarzi, Electric and Hybrid Vehicles: Technologies, Modeling and Control - A Mechatronic Approach, John Wiley & Sons Ltd, 2014.

[6] N. Sulaiman, M. A. Hannan, A. Mohamed, P. J. Ker, E. H. Majlan, W. R. Wan Daud, Optimization of energy management system for fuel-cell hybrid electric vehicles: Issues and recommendations (oct 2018). doi:10.1016/j.apenergy.2018.07.087.

[7] K. Song, F. Li, X. Hu, L. He, W. Niu, S. Lu, T. Zhang, Multi-mode energy management strategy for fuel cell electric vehicles based on driving pattern identification using learning vector quantization neural network algorithm, Journal of Power Sources 389 (2018) 230–239. doi:10.1016/j.jpowsour.2018.04.024.

[8] J. P. Gao, G. M. Zhu, E. G. Strangas, F. C. Sun, Equivalent fuel consumption optimal control of a series hybrid electric vehicle, Proceedings of the Institution of Mechanical Engineers, Part D, Journal of Automobile Engineering 223 (8) (2009) 1003–1018. doi:10.1243/09544070JAUTO1074.

[9] Y. Wang, Z. Sun, Z. Chen, Energy management strategy for battery/supercapacitor/fuel cell hybrid source vehicles based on finite state machine, Applied Energy 254 (2019) 113707. doi:10.1016/j.apenergy.2019.113707.

[10] Q. Li, W. Chen, Y. Li, S. Liu, J. Huang, Energy management strategy for fuel cell/battery/ultracapacitor hybrid vehicle based on fuzzy logic, International Journal of Electrical Power and Energy Systems 43 (1) (2012) 514–525. doi:10.1016/j.ijepes.2012.06.026.

[11] G. Zhang, W. Chen, Q. Li, Modeling, optimization and control of a FC/battery hybrid locomotive based on ADVISOR, International Journal of Hydrogen Energy 42 (29) (2017) 18568–18583. doi:10.1016/j.ijhydene.2017.04.172.

[12] A. Ferrara, S. Jakubek, C. Hametner, Energy management of heavy-duty fuel cell vehicles in real-world driving scenarios: Robust design of strategies to maximize the hydrogen economy and system lifetime, Energy Conversion and Management 232 (2021) 113795. doi:https://doi.org/10.1016/j.enconman.2020.113795.

[13] X. Wang, H. He, F. Sun, J. Zhang, Application study on the dynamic programming algorithm for energy management of plug-in hybrid electric vehicles, Energies 8 (4) (2015) 3225–3244. doi:10.3390/en8043225.

[14] O. Sundström, L. Guzzella, P. Soltic, Optimal Hybridization in Two Parallel Hybrid Electric Vehicles using Dynamic Programming, IFAC Proceedings Volumes 41 (2) (2008) 4642–4647. doi:10.3182/20080706-5-kr-1001.00781.

[15] R. Wang, S. M. Lukic, Dynamic programming technique in hybrid electric vehicle optimization, 2012 IEEE International Electric Vehicle Conference, IEVC 2012 (2012). doi:10.1109/IEVC.2012.6183284.

[16] M. P. O'Keefe, T. Markel, Dynamic programming applied to investigate energy management strategies for a plug-In HEV, 22nd International Battery, Hybrid and Fuel Cell Electric Vehicle Symposium and Exposition, EVS 2006 (November) (2006) 1035–1046.

[17] A. Panday, H. O. Bansal, Energy management strategy for hybrid electric vehicles using genetic algorithm, Journal of Renewable and Sustainable Energy 8 (1) (2016). doi:10.1063/1.4938552.

[18] C. Bordons, M. A. Ridao, A. Pérez, A. Arce, D. Marcos, Model predictive control for power management in hybrid fuel cell vehicles, 2010 IEEE Vehicle Power and Propulsion Conference, VPPC 2010 (May 2014) (2010). doi:10.1109/VPPC.2010.5729119.

[19] M. Koot, J. T. Kessels, B. de Jager, W. P. H. Heemels, P. P. van den Bosch, M. Steinbuch, Energy management strategies for vehicular electric power systems, IEEE Transactions on Vehicular Technology 54 (3) (2005) 771–782. doi:10.1109/TVT.2005.847211.

[20] G. Paganelli, S. Delprat, T. M. Guerra, J. Rimaux, J. J. Santin, Equivalent consumption minimization strategy for parallel hybrid powertrains, IEEE Vehicular Technology Conference 4 (February) (2002) 2076–2081. doi:10.1109/VTC.2002.1002989.

[21] C. Musardo, G. Rizzoni, Y. Guezennec, B. Staccia, A-ECMS: An adaptive algorithm for hybrid electric vehicle energy management, European Journal of Control 11 (4-5) (2005) 509–524. doi:10.3166/ejc.11.509-524.

[22] H. Li, A. Ravey, A. N'Diaye, A. Djerdir, Online adaptive equivalent consumption minimization strategy for fuel cell hybrid electric vehicle considering power sources degradation, Energy Conversion and Management 192 (2019) 133–149. doi:10.1016/j.enconman.2019.03.090.

[23] S. Xie, X. Hu, Z. Xin, J. Brighton, Pontryagin's Minimum Principle based model predictive control of energy management for a plug-in hybrid electric bus, Applied Energy 236 (September 2018) (2019) 893–905. doi:10.1016/j.apenergy.2018.12.032.

[24] J. Rawlings, D. Mayne, M. Diehl, Model Predictive Control: Theory, Computation, and Design, 2nd Edition, Nob Hill Publishing, LLC, 2017.

[25] Y. Al-Sagheer, R. Steinberger-Wilckens, Energy Management Controller for Fuel Cell Hybrid Electric Vehicle Based on Sat-Nav Data, Fuel Cells 20 (4) (2020) 420–430. doi:10.1002/fuce.201900196.

[26] H. Borhan, A. Vahidi, A. M. Phillips, M. L. Kuang, I. V. Kolmanovsky, S. Di Cairano, MPC-based energy management of a power-split hybrid electric vehicle, IEEE Transactions on Control Systems Technology 20 (3) (2012) 593–603. doi:10.1109/TCST.2011.2134852.

[27] Y. Huang, H. Wang, A. Khajepour, H. He, J. Ji, Model predictive control power management strategies for HEVs: A review, Journal of Power Sources 341 (2017) 91–106. doi:10.1016/j.jpowsour.2016.11.106.

[28] D. F. Pereira, F. D. C. Lopes, E. H. Watanabe, Nonlinear Model Predictive Control for the Energy Management of Fuel Cell Hybrid Electric Vehicles in Real Time, IEEE Transactions on Industrial Electronics 68 (4) (2021) 3213–3223. doi:10.1109/TIE.2020.2979528.

[29] M. Cheng, B. Chen, Nonlinear Model Predictive Control of a Power-Split Hybrid Electric Vehicle with Consideration of Battery Aging, Journal of Dynamic Systems, Measurement and Control, Transactions of the ASME 141 (8) (2019) 1–9. doi:10.1115/1.4042954.

[30] X. Hu, C. Zou, X. Tang, T. Liu, L. Hu, Cost-optimal energy management of hybrid electric vehicles using fuel cell/battery health-aware predictive control, IEEE Transactions on Power Electronics 35 (1) (2020) 382–392. doi:10.1109/TPEL.2019.2915675.

[31] L. Grüne, J. Pannek, Nonlinear Model Predictive Control Theory and Algorithms, 2nd Edition, Springer International Publishing Switzerland, 2017. doi:10.1007/978-3-030-68010-7_5.

[32] Y. Zhou, A. Ravey, M. C. Péra, Real-time cost-minimization power-allocating strategy via model predictive control for fuel cell hybrid electric vehicles, Energy Conversion and Management 229 (December 2020) (2021). doi:10.1016/j.enconman.2020.113721.

[33] Y. Zhou, A. Ravey, M. C. Péra, Multi-objective energy management for fuel cell electric vehicles using online-learning enhanced Markov speed predictor, Energy Conversion and Management 213 (December 2019) (2020). doi:10.1016/j.enconman.2020.112821.

[34] D. Zhou, A. Al-Durra, F. Gao, A. Ravey, I. Matraji, M. Godoy Simões, Online energy management strategy of fuel cell hybrid electric vehicles based on data fusion approach, Journal of Power Sources 366 (2017) 278–291. doi:10.1016/j.jpowsour.2017.08.107.

[35] Y. Zhou, A. Ravey, M.-C. Péra, Multi-mode predictive energy management for fuel cell hybrid electric vehicles using Markov driving pattern recognizer, Applied Energy 258 (January) (2020) 114057. doi:https://doi.org/10.1016/j.apenergy.2019.114057.

[36] Y. Zhou, Predictive energy management for fuel cell hybrid electric vehicle, Ph.D. thesis, UNIVERSITY BOURGOGNE FRANCHE-COMTÉ (2020).
URL https://tel.archives-ouvertes.fr/tel-03080574

[37] T. Markel, A. Brooker, T. Hendricks, V. Johnson, K. Kelly, B. Kramer, M. O'Keefe, S. Sprik, K. Wipke, ADVISOR: A systems analysis tool for advanced vehicle modeling, in: Journal of Power Sources, Vol. 110, Elsevier, 2002, pp. 255–266. doi:10.1016/S0378-7753(02)00189-1.

[38] M. J. Ogburn, Systems Integration, Modeling, and Validation of a Fuel Cell Hybrid Electric Vehicle (2000).

[39] S. D. Gurski, Cold-start effects on performance and efficiency for vehicle fuel cell systems (2002).
URL http://hdl.handle.net/10919/36290

[40] D. G. Kroger, Radiator characterization and optimization, SAE Technical Papers 93 (1984) (1984) 984–990. doi:10.4271/840380.

[41] N. S. Ap, P. Guerrero, P. Jouanny, Influence of front end vehicle, fan and shroud on the heat performance of a/c condenser and cooling radiator, SAE Technical Paper 2002-01-1206 (2002). doi:https://doi.org/10.4271/2002-01-1206.

[42] T. Fletcher, Optimal Energy Management Strategy for a Fuel Cell Hybrid Electric Vehicle, Ph.D. thesis, Loughborough University (2017).

[43] T. Fletcher, R. Thring, M. Watkinson, An energy management strategy to concurrently optimise fuel consumption and pem fuel cell lifetime in a hybrid vehicle, International Journal of Hydrogen Energy 41 (46) (2016) 21503–21515. doi:https://doi.org/10.1016/j.ijhydene.2016.08.157.

[44] H. Sadek, R. Chedid, D. Fares, Power sources sizing for a fuel cell hybrid vehicle, Energy Storage 2 (2) (2020) 1–13. doi:10.1002/est2.124.

[45] S. Onori, L. Serrao, G. Rizzoni, Hybrid electric vehicles: Energy management strategies, no. 9781447167792, Springer, London, 2016. doi:10.1007/978-1-4471-6781-5.

[46] V. H. Johnson, Battery performance models in ADVISOR, Journal of Power Sources 110 (2) (2002) 321–329. doi:10.1016/S0378-7753(02)00194-5.

[47] C. D. Stylios, P. P. Groumpos, Modeling Complex Systems Using Fuzzy Cognitive Maps, IEEE Transactions on Systems, Man, and Cybernetics Part A:Systems and Humans. 34 (1) (2004) 155–162. doi:10.1109/TSMCA.2003.818878.

[48] A. Kheirandish, F. Motlagh, N. Shafiabady, M. Dahari, A. Khairi Abdul Wahab, Dynamic fuzzy cognitive network approach for modelling and control of PEM fuel cell for power electric bicycle system, Applied Energy 202 (2017) 20–31. doi:10.1016/j.apenergy.2017.05.084.

[49] E. I. Papageorgiou (Ed.), Fuzzy Cognitive Maps for Applied Sciences and Engineering, 1st Edition, Springer-Verlag Berlin Heidelberg, 2014. doi:10.1007/978-3-642-39739-4.

[50] G. Kyriakarakos, A. I. Dounis, K. G. Arvanitis, G. Papadakis, Design of a Fuzzy Cognitive Maps variable-load energy management system for autonomous PV-reverse osmosis desalination systems: A simulation survey, Applied Energy 187 (2017) 575–584. doi:10.1016/j.apenergy.2016.11.077.

[51] A. D. Karlis, T. L. Kottas, Y. S. Boutalis, A novel maximum power point tracking method for PV systems using fuzzy cognitive networks (FCN), Electric Power Systems Research 77 (3-4) (2007) 315–327. doi:10.1016/j.epsr.2006.03.008.

[52] D. Q. Truong, J. Marco, D. Greenwood, L. Harper, D. G. Corrochano, J. I. Yoon, Challenges of micro/mild hybridisation for construction machinery and applicability in UK, Renewable and Sustainable Energy Reviews 91 (February) (2018) 301–320. doi:10.1016/j.rser.2018.03.027.

[53] J. S. Neubauer, E. Wood, Accounting for the variation of driver aggression in the simulation of conventional and advanced vehicles, SAE Technical Paper Series (2013). doi:10.4271/2013-01-1453.